A STUDY ON DAMAGE EVOLUTION MECHANISM OF HEX-CHROME FREE COATING/ALUMINUM SYSTEM AND A PROPOSED 2D TRANSMISSION LINE MODEL BASED ON EXPERIMENTAL RESULTS

A Thesis

Presented to

The Graduate Faculty of The University of Akron

In Partial Fulfillment

of the Requirements for the Degree

Master of Science

Jiani Niu

December, 2014

A STUDY ON DAMAGE EVOLUTION MECHANISM OF HEX-CHROME FREE COATING/ALUMINUM SYSTEM AND A PROPOSED 2D TRANSMISSION LINE MODEL BASED ON EXPERIMENTAL RESULTS

Jiani Niu

Thesis

Approved:	Accepted:
_____	_____
Advisor Dr. Homero Castaneda-Lopez	Dean of the College Dr. George K. Haritos
_____	_____
Committee Member Dr. Scott Lillard	Dean of the Graduate School Dr. George R Newkome
_____	_____
Committee Member Dr. Hongbo Cong	Date
_____	
Department Chair Dr. Michael Cheung	

ABSTRACT

Aluminum 2024-T3 and 7075-T6 are commonly used in aviation industry. The coating application on the aluminum surface is consider as one of the most effective method to ease the corrosion problem. Hex-chrome free coating which has less environmental issues was developed in recent years. In this work, we studied the degradation process of hex-chrome free coating/ aluminum system under the constant immersion environment with the help of a proposed damage evolution concept. This damage evolution concept includes four steps: 1. Initial water uptake process within coating layer, 2. Activation of electrochemical reaction in the coating and metal interface 3. Propagation of corrosion products below coating layer, coating delamination or degradation. 4. Coating totally fails, metal experiences severe metal loss. Three experimental variables were investigated in this project, they were: pH of electrolyte, top coat thickness, and metal effect. Impedance measurements of samples immersed in 3.5 wt% NaCl electrolyte were continually carried out for 160 days to study the impact of those experimental variables. A two dimensional transmission line model was developed in this work. This 2D-TLM was firstly verified via comparing the simulated EIS data with experimental results. A further application of this model gave us a local impedance distribution of hex-chrome free coating/aluminum profile. Via interpreting the local impedance distribution, a detailed degradation mechanism of sample in early immersion period was revealed.

ACKNOWLEDGEMENTS

First I would like to thank my advisors, Dr. Homero Castenade Lopez for his guidance and assistant in this project as well as in life. Thank you to all my colleagues and collaborators at University of Akron. An extra thank you to my thesis committee, Dr. Scott Lillard and Dr. Hongbo Cong for their comments and suggestions. Finally, I would like to thank my wonderful husband Yu Feng for his incredible support throughout my years in Akron.

TABLE OF CONTENTS

Page

LIST OF FIGURES

Figure Page

LIST OF TABLES

CHAPTER I

INTRODUCTION

1.1 Research background

Aluminum is widely used in transportation due to its good machinability, superb fatigue strength and light weight. One of the most important applications of aluminum alloys is in the aviation industry. The aluminum 2024-T3 and 7075-T6 are two of the alloys commonly used in aircraft industry due to their outstanding mechanical properties and corrosion resistance [1] however, the presence of Cu and other novel compositions in this alloy make it easier to corrode. The corrosive species in the environment such as oxygen and electrolyte can directly contact with the alloy surface to form an electrochemical galvanic cell with the aluminum as the anode and Cu as cathode result in the corrosion of the aluminum [2]. This low corrosion resistance severely threat the integrity of the aircraft structures and thus the anticorrosive treatment of aluminum alloy identified as high priority topics by the US Air Force[3].

Currently, the most common methods to alleviate the corrosion problems on the aluminum substrate are: I) adding inhibitor to the fluid environment that directly contact with substrate [4], II) apply a cathodic potential protection on the substrate material [5], and III) applying an organic coating layer on the substrate [6]; in the case of aluminum alloys used in aviation industry, the third approach is the most widely used. The applied

coating layer can protect the substrate through three main mechanisms: 1. the physicochemical (barrier), 2. The electrochemical (inhibition or cathodic protection), and 3. Adhesion mechanism [7].

Generally, the coating system consists in three layers: topcoat, primer, and pretreatment. The top coat layer works as the main barrier to protect the substrate from the corrosive factors such as oxygen, moisture and ultra-violet rays. Polyurethane is typically adopted as the top coating, and the application thickness varies from 50 to 200 pm. The primer usually contains a pigmented organic resin matrix, the thickness of this layer is about 25 μm for aircraft use. This layer improves the adhesion between coating and substrate, and slows down the transport of aggressive ion species within the polymeric structure [8]. The pretreatment layers is formed after the pretreatment process and usually it is a thin (less than 10-60 nm) inorganic layer. The pretreatment layer helps to increase the adhesion between substrate and primer layer and to protect the substrate from corrosion at the same time [9]. The complete coating system containing the three layers mentioned above is show in figure 1.1

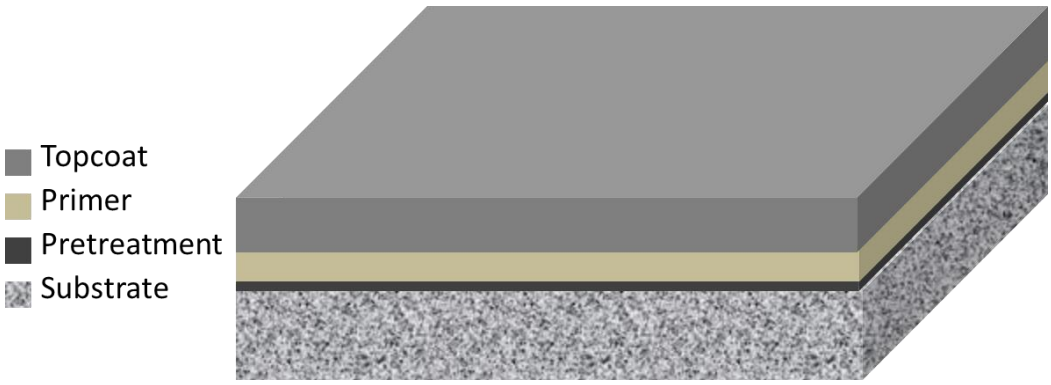

Figure 1.1 Sketch of general coating/metal system

Chromate conversion coating have been widely used as a primer; the reaction of soluble hexavalent chromium salts and chromic acid on the site of aluminum substrate generate a continuous dense layer of insoluble trivalent chromium and soluble hexavalent chromium compounds. Those compounds provide excellent adhesion to organic coating and superb corrosion resistance [10]. Despite their outstanding properties, hexavalent chromium compounds are carcinogenic and raise world-wide health concern. In recent years, with the issuing of stricter regulations regards of the low hazardous emissions, the concept of environmental friendly coating became popular, and series of the low VOC, low HAP, non-toxic coating system were established [11]. Among all those new coating products, the non-hexavalent chromium coating system brought significant attention. At the same time, in order to apply this coating system in a more economic and effective way, a deep understanding of the degradation evolution mechanism was required and thus numerous projects focus on the coating degradation topics are carried out [12].

1.2 Methods to study the coating/metal system

Depending upon the properties of the coating system we want to study, various techniques are adopted in the research. For example, coating adhesion which plays a vital

role for a successful coating application can be obtained through pressure-sensitive tape test, indentation testing, scratch test and so on [13].

The optical techniques are adopted to characterize the geometry of the targeted surface during the coating system's degradation time. For example, SEM (scanning electron microscope) and IFM (infinite focus microscopy) are used study the morphology of the sample surface[14,15]. XPS (X-ray photoelectron spectroscopy), FTIR (Fourier transform infrared spectroscopy) were used to study the composition and status of coating/metal system.[16]

Numerous electrochemical methods are adapted to monitoring the real time electrochemical properties of coating systems for investigating the detailed damage evolution mechanism[17], the simplest test is to measure the change of corrosion potential of coating/metal systems with time as well as the time dependent-potential decay studied in order to find the state of coating/metal system and predict the coating performance, however the interpretation of the experimental results are various and considered to be non-informative so far[18–20]. DC current techniques are also applied on the characterization of coating properties [21,22], via applying a dc potential pulse on the sample system, the value of the analogy electronic elements from the presumed coating model which can be determined and further used to identify the degree of damage on the coating although, there are several disadvantage of this technique: The classic Stern-Greary relation does not apply for coating systems, a correction much be made to compensate the potential drop resulted from the presence of the coating layer in order to obtain accurate results from this technique[23], besides, the coating/metal system will be destructed due to the large potential applied during the polarization process. In order to

minimize the interference brought by the measurement itself, several minimally destructive technique (MDT) or non-destructive technique (NDT) are developed[24] For example, ENM (Electrochemical noise measurement) is also used to characterize the corrosion mechanism of both bare metals and coated metals. The noise here is defined as the standard deviation of the measured sample potential. This techniques is commonly applied to study the activation stages of coating degradation and coating degradation[25,26]. AC techniques belong to the MDT and they are widely used to test the coating performance via applying a sinusoidal wave with low amplitude and specific frequency to the sample [27]. Electrochemical impedance spectroscopy (EIS) which is based on the AC technique is most commonly used these days and so adopted as the main electrochemical approach in this work. On the basic of general EIS technique, a Localized impedance spectroscopy (LIES) technique has been derived, this is a surface/interface resolution technique able to characterize the spatial and temporal activity of the sample surface to obtain the localized impedance distribution [28].

1.3 Fundamentals of EIS technique

When a steady-state system is interrupted by a small magnitude a.c voltage, it relaxes to a new state, this relaxation process provide information about the system. Impedance spectroscopy, which is the output of this technique, is defined as the ratio of applied a.c potential to response a.c current. A Laplace transformation is applied to transfer the data from time domain to frequency domain.

Generally, EIS measurement has adopted two configurations of instrumentation: Two electrode configuration and three electrode configuration. The later one is more

commonly used, the three electrodes are working electrode, reference electrode and counter electrode.

Nyquist and Bode plots are typical representation of EIS data. In order to further interpret EIS data, circuit models are developed to fit the experimental data. Randles model and models developed based on Randles are widely used as equivalent circuit models, The elements in equivalent electrical analogs describe the physical properties of each component contained in the electrochemical cell with time [29]. Classic electrochemical parameters obtained from those models are electrolyte resistance, coating resistance, coating capacitance, double layer capacitance, Warburg diffusion element and electrochemical resistance. The downside of this models are that the physical meaning of newly derived elements as well as the circuit are not clear, for example, the understanding of constant phase elements (CPEs) which can provide a better fitting compare to the pure capacitance is vague. Also, for equivalent circuits involving more than two arranged circuits, the random rearrangement of these circuits may still result in same value of impedance [30]. Last, the equivalent circuit only gives general properties of the tested sample rather than a detailed and localized physical performance. In order to interpret EIS data in a more precise way, modeling, such as transmission line modeling, is used to embraced and improve this work.

1.4 The development of transmission line model

The concept of transmission line model is first proposed by Lord Kelvin, Oliver Heaviside et.al and applied on the 1855 trans-Atlantic submarine telegraph cable project to predict the cable performance. Mathematical analysis helps the development of the

transmission line model and enables the application in the electrochemical systems. In 1905, the transmission line model was firstly used to understand the electrochemical behavior during the simulation of membranes. Later, the transmission line model was adopted to study the roughness and porosity of electrodes by deLevie and his group. They also simulated battery electrodes, corroding rebar in concrete, electro-catalysts, corrosion of carbon steel in high temperature aqueous systems, and super-capacitors via transmission line model. in recently years, the transmission line model was extensively studied, Macdonald and his group divided the transmission line into infinitesimally small elements applying Kirchoff's and Ohm's laws and then integrate along the line to obtain the impedance of a porous electrode, thus monitoring the evolution of the number of active pores in the electrode; the transmission line model was also used to obtain the impedance distribution of pores in an iron oxide layer (hematite) [31]. As well as characterizing porous electrodes [32] and iron oxide layers with varying oxygen-iron ratios [33].

In general, Transmission line modeling (TLM) appears to be a powerful method to identify and quantify interfacial mechanisms at different scales for porous electrodes and to elucidate corrosion mechanisms occurring at the working electrode [34]. TLM offers a better interpretation of the EIS data and gives a more detailed electrochemical degradation mechanism of coating/ metal system.

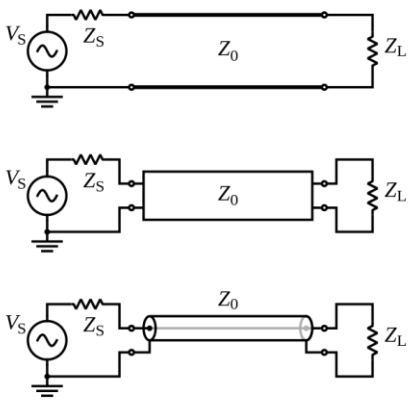

Figure 1.2 Configuration of transmission line

1.5 Summary of previous work

Numerous works have been done to investigate the damage evolution mechanism for coating/metal system. qualitative analysis of the deterioration of organic coatings and the bonding between coatings and metals under several exposure conditions has been carried out [35]. For example, Deflorian et al. [36] studied the effect of environmental factors, such as UV exposure, temperature and humidity; whereas Akbarinezhad et al. [37] investigated the variation in coating resistance and capacitance during coating chemical degradation. In addition, Walter [38] studied the effects of water uptake and chloride ion concentration on the degradation of coating/metal systems, and Haruyama et al [39] analyzed the delamination ratio of coatings by determining the breaking point frequency.

In addition, due to the accelerated experimental test as well as extended testing periods, single stages in the whole degradation process are investigated in details but separately. For instance, continuous and parallel processes related to the electrolyte uptake within coating layer which is also consider as the initial degradation of coatings are carried out [40]; the significance of the charge transfer mechanism during the metallic

dissolution process have also been studied [41]. The formation of blistering and the delamination mechanism were hot research topics as well [42].

Based on the previous work, we proposed a damage evolution concept for coating/metal system that includes four stages: stage-I, mass transfer process within coating process; stage-II, the initialization of electrochemical reaction in the coating/metal interface; stage-III, the charge transfer dominating process; stage-IV, coating failure stage. Figure 1.3 is a schematic representation of the damage evolution concept. In stage I, the corrosive ions transfer from the aqueous environment to the coating layer, water is the media in this process. Stage II begins when the corrosive species penetrate the coating layer and react with the metal substrate. In the third stage, the electrochemical reaction in the coating/substrate interface become the predominate process impacting the corrosion process, the propagation of corrosion products later will results in the coating delamination and the coating will be degrade by the corrosive environment as well. In the final stage, the coating totally fails and cannot perform protective function. The metal substrate directly contact with the corrosive environment and suffers severe metal loss.

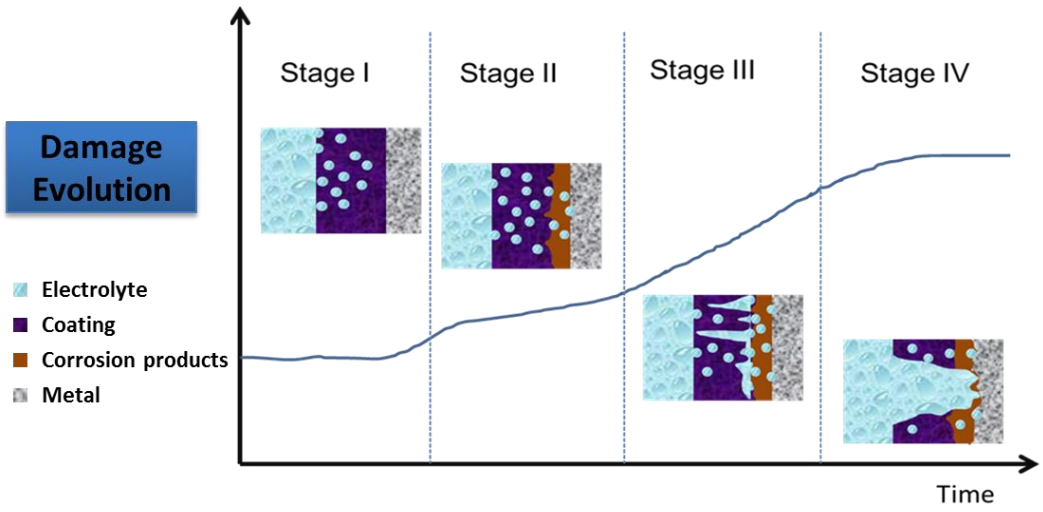

Figure 1.3 Sketch of damage evolution concept

1.6 Work Highlights

In this work, we selected a hex-chrome free coating/aluminum system, the combination of Fluoropolyurethane epoxy based topcoat and epoxy primer are consider as the environmental friendly coating layer applied on two substrates: aluminum alloys 2024-T3 and 7075-T6. The coated system was immersed in 3.5 wt% NaCl electrolyte at three different pH (pH =4.0, 7.0, 10.0) for 160 days. A three-electrode arrangement was designed to obtain the EIS spectra of this system in function of time. Both, Nyquist and Bode plots for each EIS spectra are presented in this work and interpreted in general with the reference of previous work.

In order to have a more detailed understanding about the performance/damage evolution of this system, we proposed a two dimensional transmission line model; this model is able to present the impedance distribution profile and reveals the local

degradation mechanism associated with the coating/aluminum system. A sensitivity analysis is also introduced in this work to show the impact of the magnitude and location of model variables on the simulated EIS spectra.

CHAPTER II

EXPERIMENTAL DESIGN

2.1 Sample preparation

In this work, both aluminum alloys 2024-T3 and 7075-T6 were used as substrate; Table 2.1 present the compositions of these alloys. The suffix T3 and T6 indicate two post thermal treatment processes; in the T3 method, the aluminum is first treated with solution, heated and then cold worked. In the T6 treatment, the aluminum is solution treated and then it is subject to an aging process. In general, alloy through T3 treatment is mechanically superior to T6 product.

Table 2.1 Composition of AA 2024-T3 and AA 7075-T6

Component	AA 2024-T3	AA 7075-T6
Al	90.7-94.7	87.1-91.4
Cr	< 0.10	0.18-0.28
Co	3.80-4.90	1.20-2.00
Fe	< 0.50	< 0.50
Mg	1.20-1.80	2.10-2.90
Mn	0.30-0.90	< 0.30
Si	< 0.50	< 0.40
Ti	< 0.15	< 0.20
Zn	< 0.25	5.10-6.10
other	< 0.15	<0.15

AA2024-T3 and AA7075-T6 substrates in the form of a panel were cleaned with acetone prior to coating application. The panels were then mounted on cardboard before coating application.

An epoxy primer (Deft 02Y040) and a hex-chrome free polyurethane topcoat (Deft 99GY010) were used in this work. Both, the primer and the topcoat included two components (resin/cross linker). Those two components were blended and mixed for one minute at 1700 RPM on a Flacktek Speedmixer. The mixed coatings were given an induction time of 20-30 minutes prior to application. After the induction time, coatings were applied with a high volume low pressure (HVLP) spray gun at the target wet film thicknesses specified. Approximate 0.023 mm primer was achieving directly above the substrate, a layer of top coat was then accomplished upon the primer. The top coat thickness is well controlled and studied as an experimental variable. We presented the detailed matrix in section 2.4

2.2 Experimental setup

As indicated in Figure 2.1, a glass cell was clamped on the surface of the coated sample, an acrylic plate was placed under the coated sample to support the sample from bending. A rubber ring was used to seal the space between the coated sample and glass cell. The sample area within the sealed glass cell is about 4.52 cm^2.

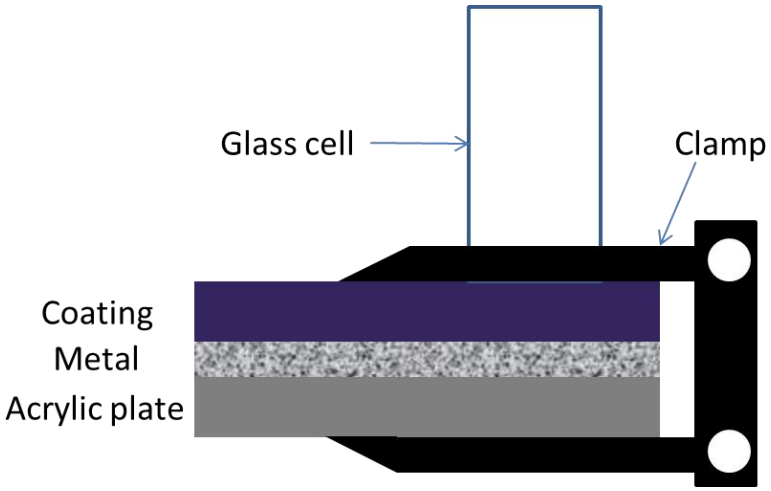

Figure 2.1 Sketch of glass cell clamped above the coated sample

Before the experiments, the glass cell was filled with electrolyte and the sample area with the sealed region is in constant immersion at room temperature. Figure 2.2 is the experimental set up for constant immersion test.

The electrolyte was 3.5 wt.% NaCl solution with steady pH (4.0, 7.0, 10.0). The pH was fixed using buffer chemical which is another experimental variable we would study. The matrix was presented in section 2.4 as well.

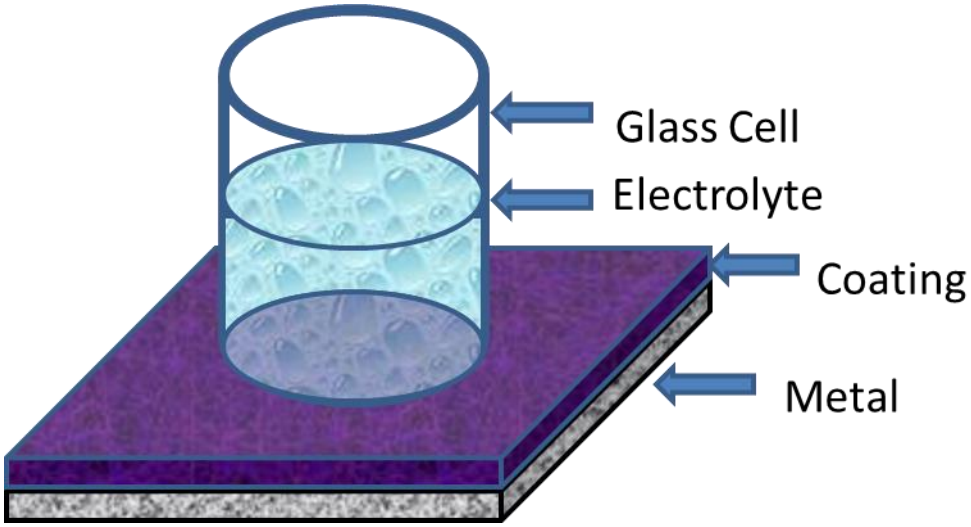

Figure 2.2 Experimental setup for constant immersion test

2.3 Control parameters studied in this work.

In this work, we investigated the impact of the solution pH, topcoat thickness and metal substrate on damage evolution mechanism respectively.

Table 2.2 is the chemical buffer adopted in this work to maintain the electrolyte pH; 0.1 M solutions of each buffer chemicals were prepared first. Via adding the buffer solution into the 3.5% wt. NaCl solution, we obtained the electrolyte with controlled pH (pH=4.0, 7.0, 10.0)

Table 2.2 Buffer chemicals used to control the electrolyte pH

pH	Chemical 1	Chemical 2
4	Acetic acid	Sodium Acetate
7	Disodium hydrogen phosphate	Hydrochloric acid
10	Disodium hydrogen phosphate	Sodium hydroxide

The second parameter we studied in this work is the topcoat thickness. The coating system we adopted in this work is a combination of primer and topcoat, the primer was achieved with a thickness of 0.023 mm. Three topcoat thicknesses were investigated in this work and they are indicated in Table 2.3

Table 2.3 Three topcoat thickness used in this work

No	Topcoat thickness
Coating-1	0.025mm
Coating-2	0.050mm
Coating-3	0.075mm

2.4 Electrochemical impedance measurement

EIS measurements were performed in a three-electrode electrochemical cell as show in figure 2.3. Metal/coating samples were used as the working electrode, a saturated calomel electrode (SCE) was used as the reference electrode, and a platinum mesh served as the counter electrode.

A Gamry Reference 600TM was used to perform the EIS and open-circuit potential measurements. The EIS data were collected over a frequency range from 1 mHz to 20 kHz with a voltage amplitude of ±10 mV from the corrosion potential. The data acquisition was controlled by Gamry Framework Version 5.8/EIS 300 software. All the measurements were performed at room temperature.

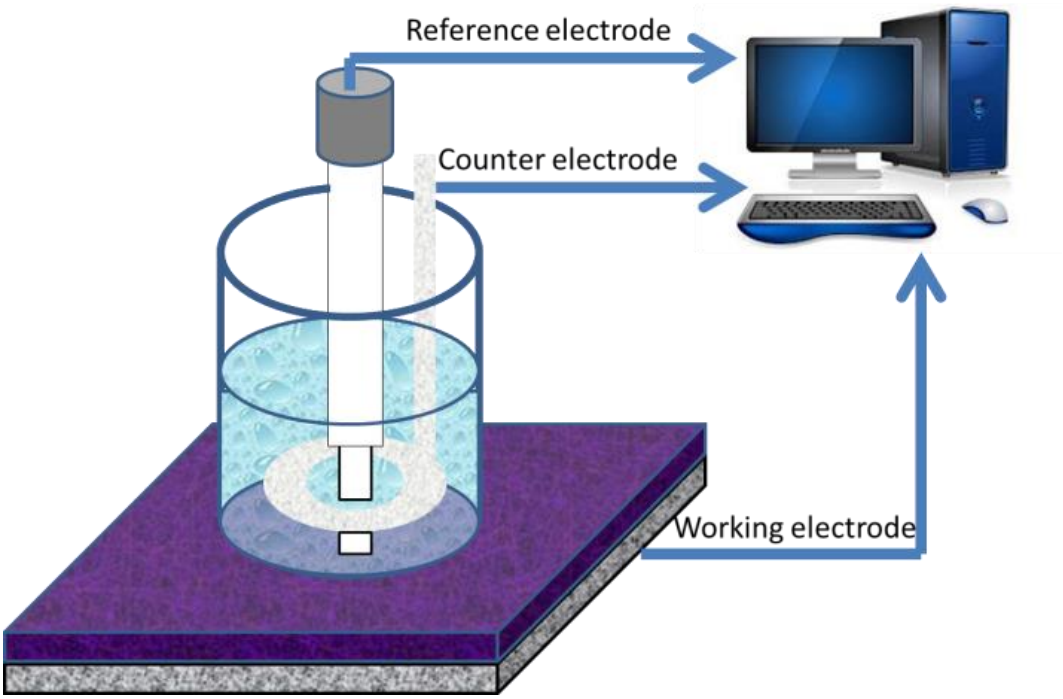

Figure 2.3 Electrochemical impedance measurement setup

CHAPTER III

PROPOSED 2D TRANSMISSION LINE MODEL THEORY

Transmission line modeling (TLM) has been extensively used to study the electrochemical activities on porous interface. Figure 3.1 is a sketch of general transmission line model. As showed in figure, a transmission line was divided into a sequence of n-1 segments. Each segment contained four impedance elements and considered as an electrical circuit loop by itself as well. The current direction is indicated in arrows in the figure. Depend on the scenario, the impedance elements from different segments can have either same or different expression. For instance, we applied the TLM from figure 3.1 on the study of pipeline corrosion; Assume the pipeline was alone the x direction as well, if the pipeline was intact, all the impedance elements that describe the physical properties of the pipeline would be the same ($Z_1=Z_2=\ldots=Z_{n-1}=Z_n$). If the pipeline was partially corroded, the impedance elements that used to describe the physical properties would have different expression depend on the location of the impedance elements in the TLM.

In general, we were able to describe the local electrochemical behaviors of studied interface via assigning specific impedance expression for each segment. we named those impedance elements as localized impedance since all the impedance has its own physical meaning and expression depend on its location. Usually, the expression of

localized impedances in includes the solution resistance, the resistance of the conducting substrate and the interfacial impedance [43].

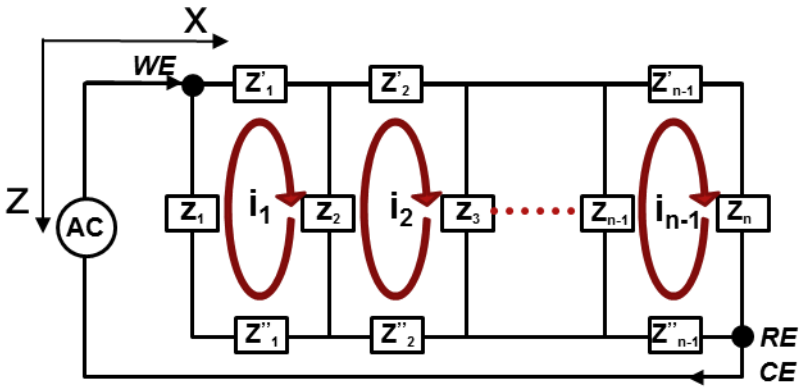

Figure 3.1 Sketch of general transmission line model

The magnitude of each local impedance Z will be determined with the help of equivalent circuit analogy [44]. The local electrochemical mechanism would be disclosed upon the analysis of the local impedance distribution.

In this work, a two dimensional transmission line model was proposed; Figure 3.2 is the electronic element representation of the proposed 2D transmission line model. In this model, the main circuit was divided into a $n \times m$ matrix segments. We were able to see a more detailed impedance distribution in two mutually perpendicular directions instead of one direction as in previous models. The current path as well as the local current in each segment was also indicated in blue arrow in figure 3.2.

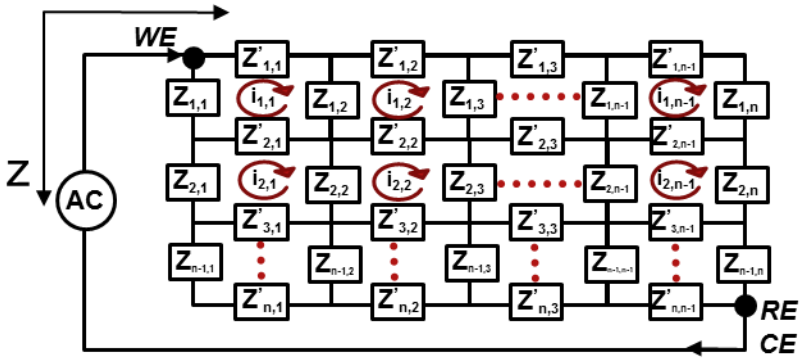

Figure 3.2 Sketch of 2D transmission line model

According to the Kirchhoff's voltage law, the sum of the voltage difference in any closed network is zero, and if we assign a voltage for each segment in the model, equation 1 is valid.

$$\sum_{k=1}^{n} V_k = 0 \tag{1}$$

Where V_k is the local voltage for k^{th} segment.

We noticed that the voltage in each segment is zero, thus, a relation between current and impedance in each segment was derived based on Kirchhoff's voltage law. For example, for the segment in the location of 1×1 in figure 3.2, we obtained the relation between local impedance elements and local current as follows

$$I_{1,1}\left(Z_{1,1} + Z_{1,2} + Z'_{1,1} + Z'_{2,1}\right) - I_b \times Z_{1,1} - I_{2,1} \times R_{2,1} - I_{1,2} \times Z_{1,2} = 0 \tag{2}$$

Similarly to equation 1, we can find an equation describing the relation between the local impedance elements and the current for each segment. In this way, we can obtain an equation set containing each equation describing the relation between the local impedance with its correspondent local current for one specific segment. The equation set is indicated below.

$$I_{1,1}\left(Z_{1,1}+Z_{1,2}+Z'_{1,1}+Z'_{2,1}\right)-I_b\times Z_{1,1}-I_{2,1}\times Z'_{2,1}-I_{1,2}\times Z_{1,2}=0$$

$$I_{1,2}\left(Z_{1,2}+Z_{1,3}+Z'_{1,2}+Z'_{2,2}\right)-I_{1,1}\times Z_{1,2}-I_{1,3}\times Z_{1,3}-I_{2,2}\times Z'_{2,2}=0$$

$$\vdots$$

$$I_{n,m-1}\left(Z_{n-1,m-1}+Z_{n-1,m}+Z'_{n-1,m-1}+Z'_{n,m-1}\right)-I_b\times Z'_{n,m-1}-I_{n-1,m-1}\times Z'_{n-1,m-1}=0$$

The magnitude of each local impedance and resistance was assigned from equivalent circuit analogy. We considered them as known variables. In order to solve the equation set presented above, Matrix algebra method is adopted here in the form of A**X**=b, where

$$\mathbf{A}=\begin{pmatrix} Z_{1,1}+Z_{1,2}+Z'_{1,1}+Z'_{2,1} & -Z_{1,2} & 0 & \cdots & -Z'_{1,2} & 0 & \cdots & 0 \\ -Z_{1,2} & Z_{1,1}+Z_{1,2}+Z'_{1,2}+Z'_{2,2} & -Z_{1,3} & \cdots & 0 & -Z'_{2,2} & \cdots & 0 \\ \vdots & \vdots & \vdots & & & \ddots & & \\ 0 & 0 & 0 & \cdots & Z_{n-1,m-1}+Z_{n-1,m}+Z'_{n-1,m-1}+Z'_{n,m-1} & \cdots & -Z'_{n-1,m-1} & \end{pmatrix}$$

$$\mathbf{x}=\begin{pmatrix} i_{1,1} \\ i_{1,2} \\ \vdots \\ i_{n-1,m-1} \end{pmatrix} \qquad \mathbf{b}=\begin{pmatrix} i_b Z_{1,1} \\ 0 \\ \vdots \\ i_b Z''_{n,m-1} \end{pmatrix}$$

By solving this matrix, we obtained the matrix of **X** which is the current distribution of the sample area. One thing we would like to emphasize is that the current

distribution calculated with the above method is under one single specific frequency and an iterative method would account for all the frequency range proposed. Then, the total impedance of the sample area under that specific frequency was further obtained by equation (3)

$$Z_{total}(\omega) = \sum_{k=1}^{n-1} Z_{k,1} + \sum_{j=1}^{m-1} Z'_{n,j} - \left(\sum_{k=1}^{n-1} \frac{Z_{k,1} * i_{k,1}}{i_b} + \sum_{j=1}^{m-1} \frac{Z'_{n,j} * i_{n-1,j}}{i_b}\right) \quad (3)$$

As indicated in equation 3, each frequency possesses one total impedance for the whole study area; by computing the total impedances for each frequency ranges from 20KHz to 10 MHz, a set of simulated impedance behavior could be obtained from this 2D transmission line model.

CHAPTER IV

EXPERIMENTAL RESULTS

Immersion experiments were carried out to study the effects of electrolyte pH, topcoat thickness and substrate type on the damage evolution process for hex-chrome free coating/aluminum system. EIS technique was used to study the damage evolution mechanism in this work.

4.1 pH effect

The first variable studied in this work is the pH effect, hex-chrome free coating (with 1 mil topcoat thickness)/aluminum 2024-T3 system was immersed in 3.5 wt.% NaCl solution with controlled pH for 160 days. The buffer chemicals used to control the pH were also presented in table 2.2

The experimental matrix in presented in table 4.1 and Figures 4.1-4.6 present the Nyquist and Bode plots for the system in pH 4.0, 7.0, 10.0 respectively.

Table 4.1 Experimental matrix to study the pH effect

tested system	variable
hex-chrome free coating(1 mil topcoat thickness)/AA 2024-T3	3.5 wt. % NaCl solution with pH 4.0
	3.5 wt. % NaCl solution with pH 7.0
	3.5 wt. % NaCl solution with pH 10.0

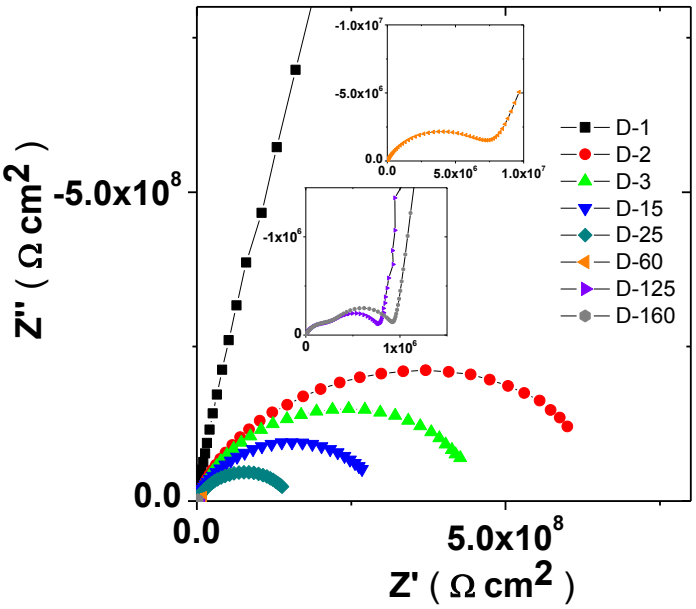

Figure 4.1 Nyquist representation of hex-chrome free coating (1mil)/aluminum 2024-T3 system immersed in 3.5 wt % electrolyte pH 4.0 for 160 days

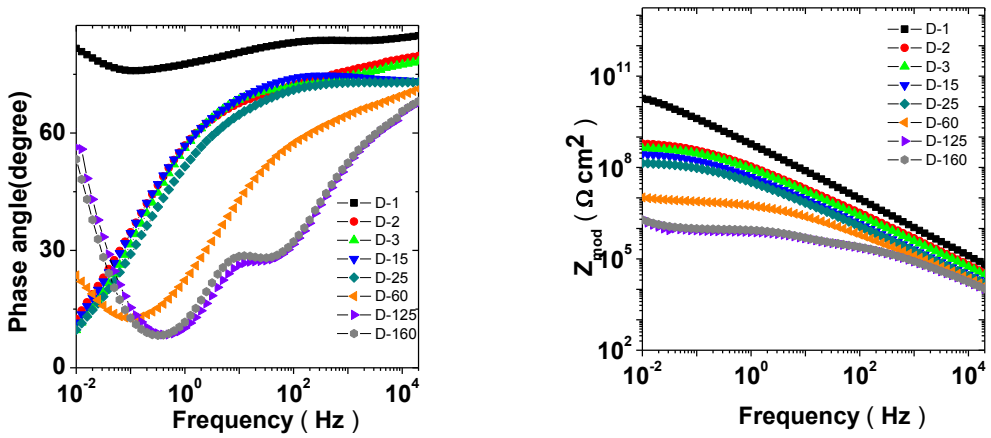

Figure 4.2 Bode representation of hex-chrome free coating (1mil)/aluminum 2024-T3 system immersed in 3.5 wt % electrolyte pH 4.0 for 160 days

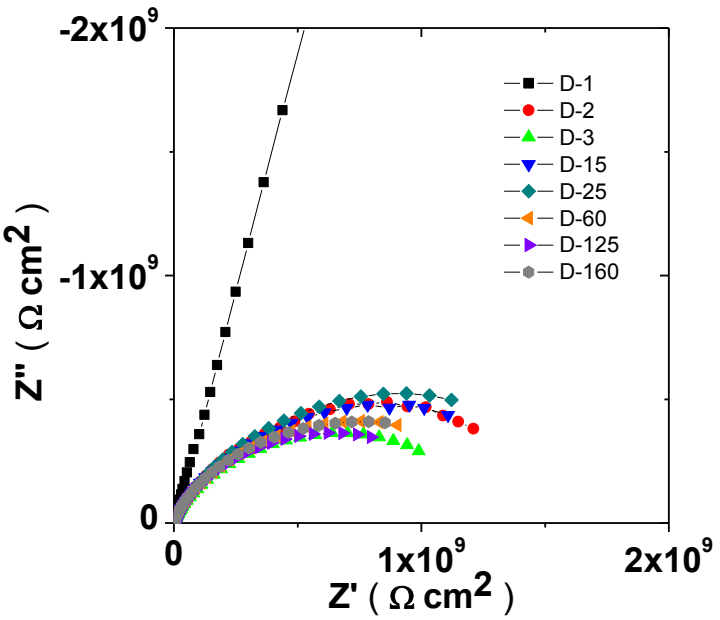

Figure 4.3 Nyquist representation of hex-chrome free coating (1mil)/aluminum 2024-T3 system immersed in 3.5 wt % electrolyte pH 7.0 for 160 days

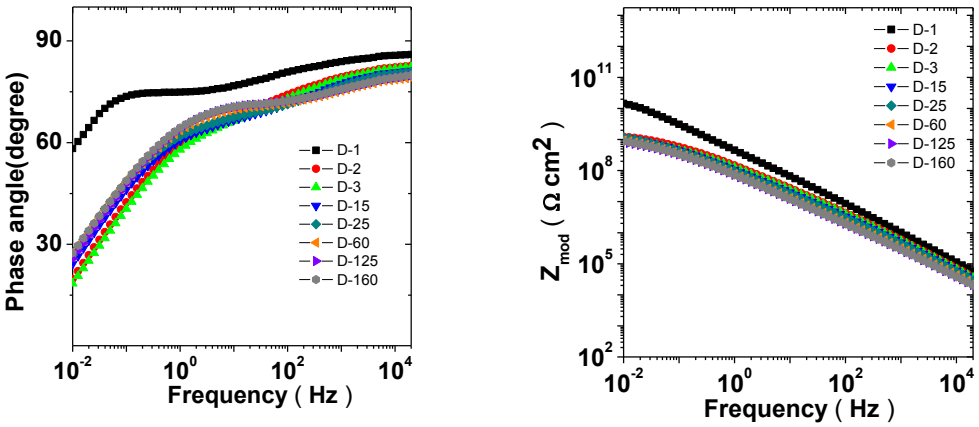

Figure 4.4 Bode representation of hex-chrome free coating (1mil)/aluminum 2024-T3 system immersed in 3.5 wt % electrolyte pH 7.0 for 160 days

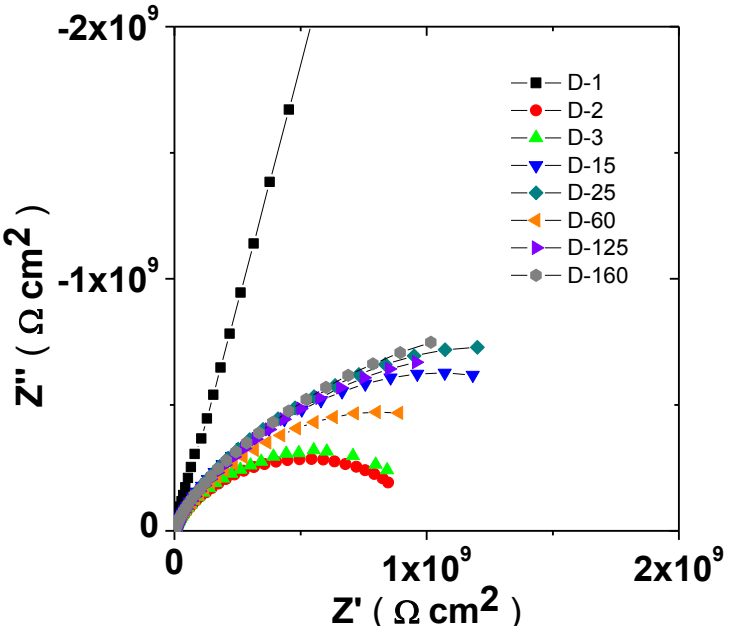

Figure 4.5 Nyquist representation of hex-chrome free coating (1mil)/aluminum 2024-T3 system immersed in 3.5 wt % electrolyte pH 10.0 for 160 days

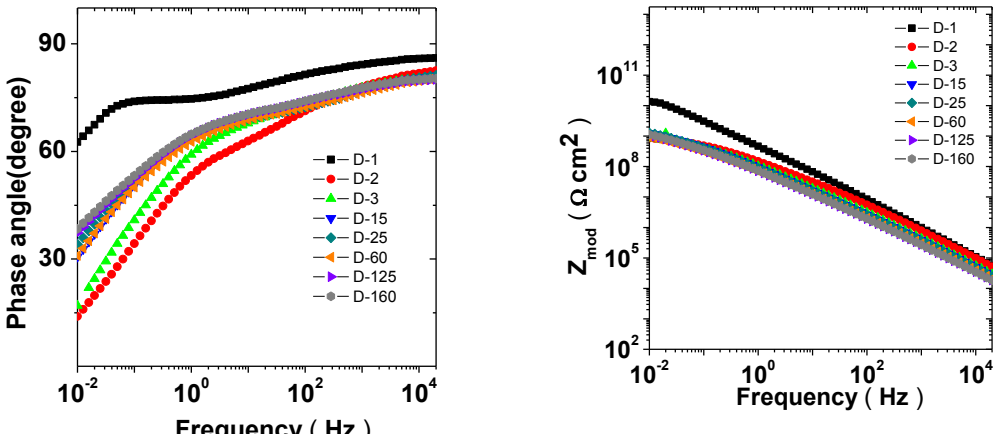

Figure 4.6 Bode representation of hex-chrome free coating (1 mil)/aluminum 2024-T3 system immersed in 3.5 wt % electrolyte pH 10.0 for 160 days

For the initial immersion time, the EIS spectra appear similar for samples immersed in all three electrolyte condition. According to the Nyquist plot, coatings behave as excellent capacitor in the initial immersion time. We consider coating is under intact dry conditions at the start time. For further days, a considerable difference appeared in the EIS spectra for coated sample under various pH electrolytes.

For the system immersed in pH 4.0 electrolyte, the radius of the capacitive loop kept decreasing from the first day to the end of the testing time. At day 60, a small tail observed in the low frequency range (10^{-1}-10^{-2} Hz) in the Nyquist plot indicated the activation of electrochemical reaction at the coating/substrate interface. The tested system transited into stage II of damage evolution process. In day 125, the magnitude of the impedance decrease to 10^5 ohm-cm^2 and three time constants appeared in the EIS spectra; the one appearing at high frequency range (10^2-10^4 Hz) was attributed to the coating layer, the one showed at medium frequency range (10^0-10^2 Hz) resulted from the electrical double layer effect, and the time constant in the low frequency range (10^{-2}-10^0 Hz) was attributed to the newly formed oxide products. According to the Nyquist spectra, a pure capacitor behavior was observed in the low frequency range (10^{-2}-10^0 Hz). It suggested the newly formed oxide products layer is a compact layer which insulates the substrate from the corrosive species to some extent.

In the case of the sample immersed in pH 7.0 electrolyte, the magnitude of the impedance as well as the shape of the EIS spectra did not change too much during the experiment. The magnitude of the impedance remains around 10^9 ohm cm^2 indicating that the coating performance excelled for the designed coating/aluminum system. Only one time constant was observed during the immersion period; this time constant resulted

from the electrolyte transport process within the coating layer. The EIS spectra suggested there was no electrochemical reaction occurring at the coating/metal interface during the whole immersion time. The tested system was still under stage I of damage evolution process up to 160 days in 3.5 wt% NaCl pH 7.0 electrolyte.

For coating system immersed in pH 10.0 electrolyte: only one time constant was observed in medium and high frequency range, no electrochemical reaction in the coating/aluminum interface was indicated by EIS spectra. The tested system is also on stage I of damage evolution process. Nevertheless, a small increment in the magnitude of the impedance was observed in the Nyquist representation from day 3, this might be attributed to the reaction between the polymer coating and the alkali electrolyte: The reaction products form a structure which exerted a protective function and impacted the EIS spectra.

In conclusion, we found the 3.5% NaCl solution at pH 4.0 simulated the most aggressive environment compared to the other two pH electrolyte for hex-chrome free coating/aluminum system. The coating was degraded faster under pH 4.0 electrolyte environment which allowed the penetration of corrosive species such as oxygen and water through the coating layer, the electrochemical reaction was activated since plenty amount of corrosive species reached the substrate. With the continued electrochemical reaction, the substrate suffers metal loss and reflected on the EIS spectra with a lower magnitude impedance. Nevertheless, corrosion products formed a condensed stabled oxide layer above the substrate which slowed down the corrosion rate in some extent.

4.2 Layering effect

In this section, we studied the impact of topcoat thickness on the damage evolution process. As described in section 2.4, coating/aluminum 2024-T3 with various top coat thickness (1mil, 2mil, and 3mil) were investigated. Table 4.2 is the experimental matrix we used to study the layering effect

Table 4.2 Experimental matrix to study the topcoat thickness

tested system	variable
hex-chrome free coating/AA 2024-T3 in 3.5 wt% NaCl pH 4.0 electrolyte	topcoat thickness 1mil
	topcoat thickness 2mil
	topcoat thickness 3mil

3.5 wt% NaCl solution pH 4.0 was used as the electrolyte in this study. This electrolyte simulated the most aggressive environment which was proved by section 4.1. We were able to observe the typical electrochemical behavior of tested samples in several stages within 160 days of immersion in this electrolyte. EIS analysis were carried out for a qualitative study of the layering effect. Figure 4.7-4.10 are the Nyquist and Bode representations of the EIS spectra for hex-chrome free coating (2mil, 3mil topcoat thickness respectively)/aluminum 2024-T3 system immersed in 3.5% wt NaCl pH 4.0 electrolyte for 160 days. The EIS spectra for hex-chrome free coating (1 mil topcoat thickness)/aluminum 2024-T3 system immersed in 3.5 wt% NaCl pH 4.0 electrolyte for 160 days was already presented in figure 4.1-4.2.

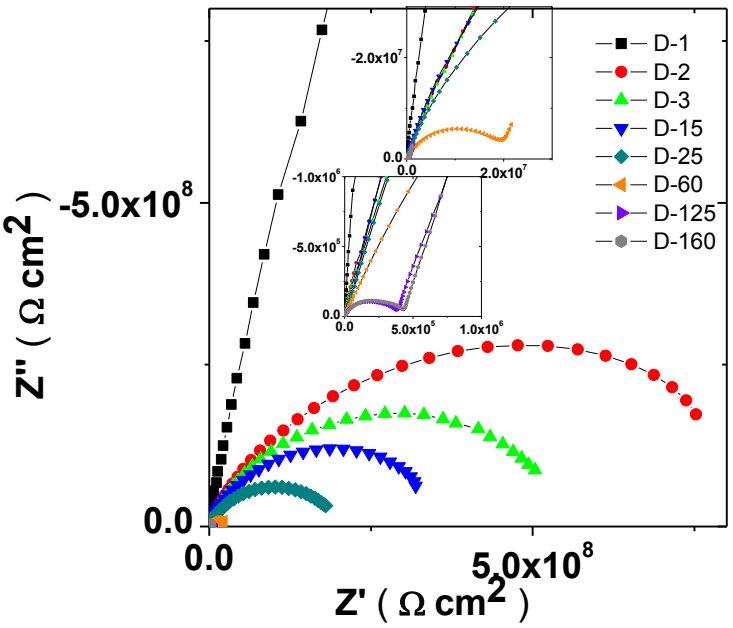

Figure 4.7 Nyquist representation of hex-chrome free coating (2 mil)/aluminum 2024-T3 system immersed in 3.5 wt % electrolyte pH 4.0 for 160 days

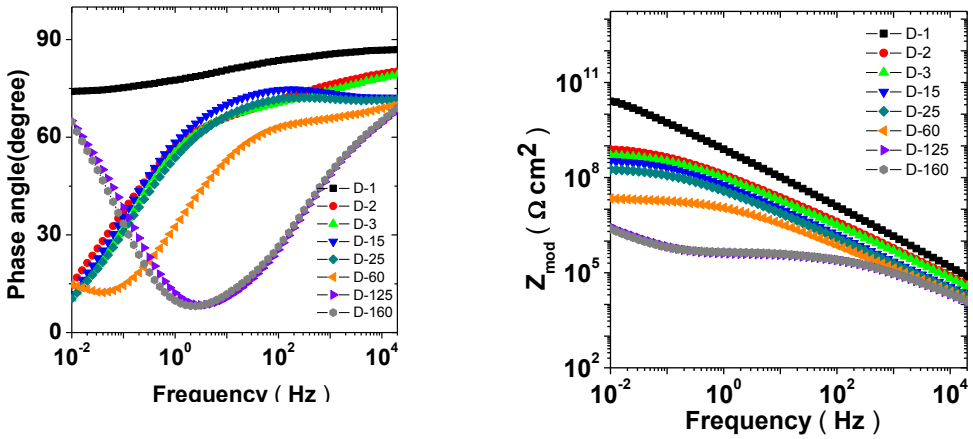

Figure 4.8 Bode representation of hex-chrome free coating (2 mil)/aluminum 2024-T3 system immersed in 3.5 wt % electrolyte pH 4.0 for 160 days

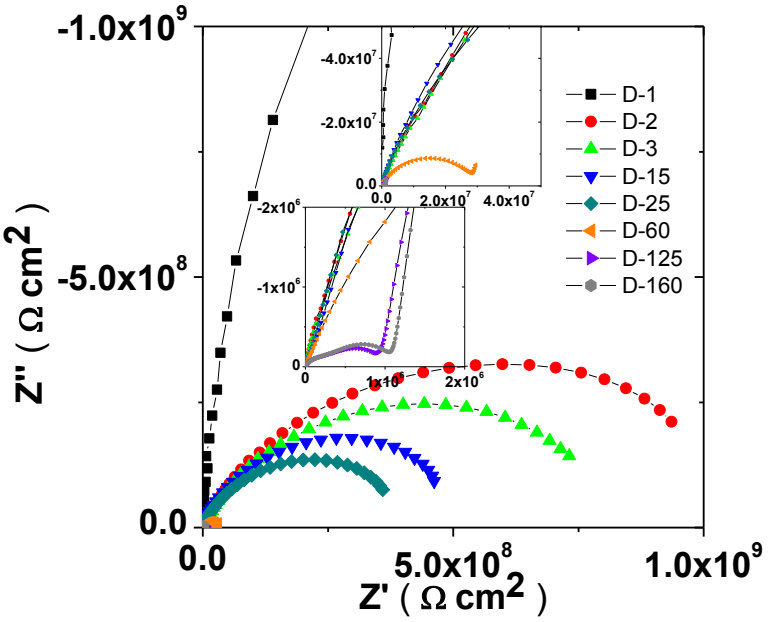

Figure 4.9 Nyquist representation of hex-chrome free coating (3 mil)/aluminum 2024-T3 system immersed in 3.5 wt % electrolyte pH 4.0 for 160 days

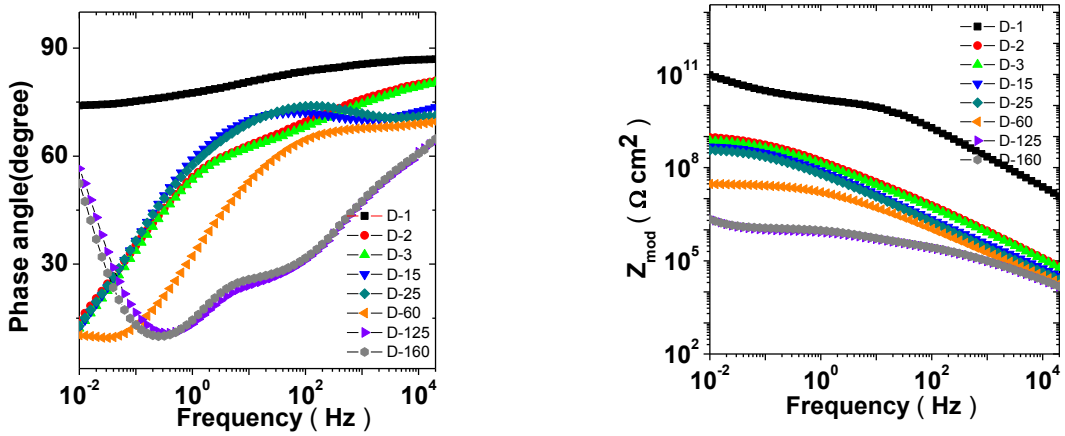

Figure 4.10 Bode representation of hex-chrome free coating (3 mil)/aluminum 2024-T3 system immersed in 3.5 wt % electrolyte pH 4.0 for 160 days

By comparing the EIS data of all three cases, we found the general trend in EIS spectra were similar: in the initial time, the coating behaves as an excellent capacitor which suggested the coating was under intact and dry condition. The magnitude of impedance decreased from day 2 for all tested systems, this suggests that the electrolyte was being uptaken the coating layer from day 2. Besides, a small tail was observed in the low frequency range (10^{-1}-10^{-2} Hz) in the Nyquist representation on day 60 for all three topcoat systems. This impedance behavior indicated the beginning of electrochemical reaction at this point. All the tested coating/alloy systems were in stage II of damage evolution process. Three time constants were observed on day 125, the newly formed time constant in low frequency range was attributed to the layer formed by the products of electrochemical reaction (corrosion products). Besides, a diffusion-like behavior in the low frequency indicated the newly form layer is porous and diffusion within the layer is the predominant process to control the corrosion rate and thus reflected on the EIS spectra as well.

However, there is still slight difference in EIS spectra for the three tested system: for the same immersion time (take day 2 as example), the magnitude of impedance differs, it has the following relations: $Z_{1mil}<Z_{2mil}<Z_{3mil}$. This trend was observed in other dates as well. In general, we found that increasing the top coat thickness in the range of 1mil to 3mil will not significantly affect the corrosion mechanism; nevertheless, the magnitude of impedance for different tested sample system suggested the system with thicker topcoat has a slight better protective function compare to the system with thinner topcoat.

4.3 Substrate effect

The impact of substrate on the degradation mechanism of coating/alloy system were studied as well in this work. Aluminum 2024-T3 and aluminum 7075-T6 were used as the tested substrate. Table 4.3 is the experimental matrix used to study the substrate effect.

Table 4.3 Experimental matrix to study the substrate effect

tested system	variable
hex-chrome free coating(1mil)/substrate in 3.5 wt% NaCl pH 4.0 electrolyte	substrate AA2024-T3
	substrate AA7075-T6

3.5% wt NaCl pH 4.0 solutions were consider as the electrolyte in this study for the same reason mentioned in section 4.2. EIS measurements were carried out for the tested sample immersed in the electrolyte during 160 days.

Figure 4.11-4.12 are the EIS spectra of hex-chrome free coating (1mil)/AA7075-T6 system immersed in 3.5 wt% NaCl pH4.0 electrolyte for 160days. The EIS spectra of hex-chrome free coating (1mil)/AA2024-T3 system immersed in 3.5 wt% NaCl pH4.0 electrolyte for 160days was already presented in figure 4.1-4.2

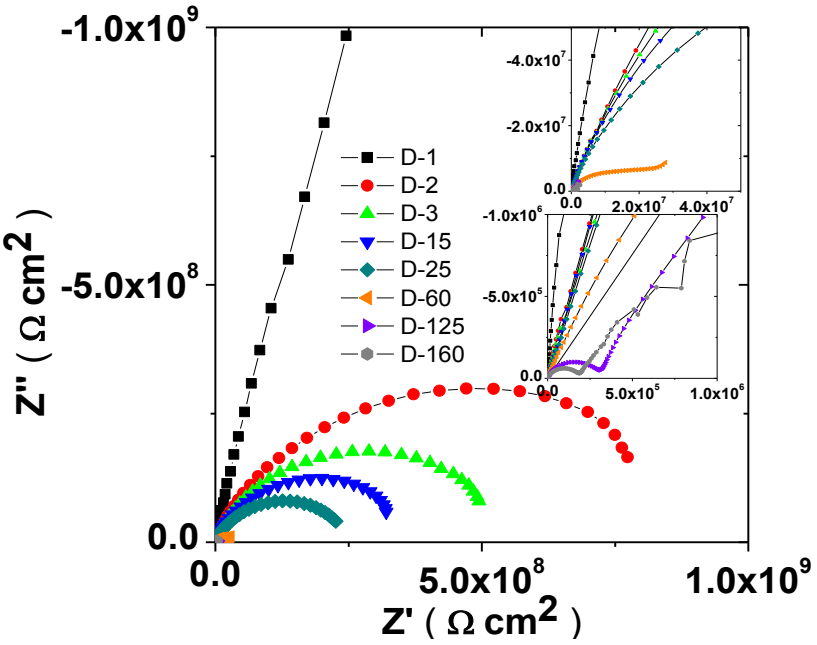

Figure 4.11 Nyquist representation of hex-chrome free coating (1 mil)/aluminum 7075-T6 system immersed in 3.5 wt % electrolyte pH 4.0 for 160 days

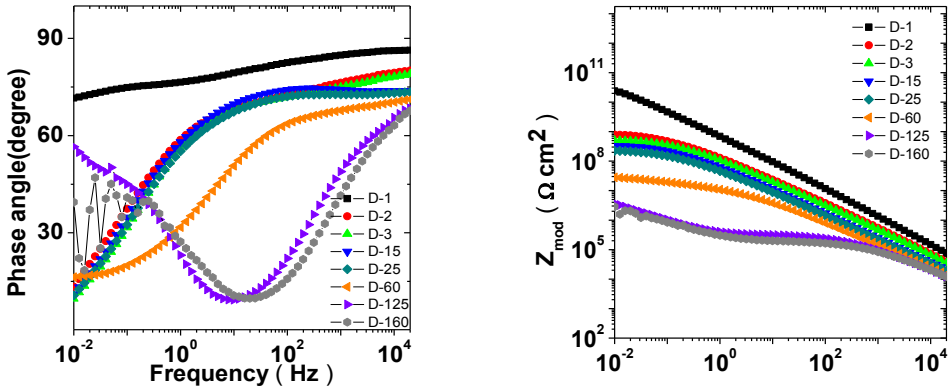

Figure 4.12 Bode representation of hex-chrome free coating (1 mil)/aluminum 7075-T6 system immersed in 3.5 wt % electrolyte pH 4.0 for 160 days

As showed in the impedance spectra, the impedance behavior for the first 25 days are similar, at which the system is still under stage I of damage evolution process. The initialization of electrochemical reaction was observed on day 60 for both test systems.;

this indicates that the electrolyte uptake process within the coating layer was not affected by the different substrate. On day 125, at which the electrochemical reaction was significant and metal substrate was experiencing metal loss, the magnitude of the impedance for the coating/aluminum 7075-T6 is smaller than the one for coating/aluminum 2024-T3 system. This observation suggested that the aluminum 7075-T6 is more susceptible to corrode compare to the aluminum 2024-T3 in this specific environment.

CHAPTER V

APPLICATION OF TRANSMISSION LINE MODEL IN COATING/ALUMINUM SYSTEM

In this section, the results of the 2D transmission line model developed in chapter III when applied to the experimental system (hex-Chrome free coating/2024-T3 aluminum substrate system constantly immersed in 3.5.wt% NaCl solution with pH 4.0) are analyzed.

Figure 5.1-a shows the lateral view of the coating/aluminum system, the system is comprised of three layers: electrolyte layer, coating layer and the substrate layer. In order to apply the 2D transmission line model, first, it is assumed that the coating/aluminum system reached steady state and each layer is uniformly distributed in horizontal level. Figure 5.1-b is the transmission line representation applied to the lateral view. As indicated in the figure, each layer has its own impedance representation, and each impedance representation has its own equivalent analogy to describe the physical significance of each layer. The total impedance for the whole system can be calculated according to equation 3.

At the same time that the local impedance distribution generated by the 2D TLM describes the local electrochemical properties of the coating/aluminum system, the change of local impedance distribution provides the detailed information of water uptake

process and electrochemical reaction process. Both features are key processes impacting the degradation mechanism in coating/aluminum system[35,46]. to achieve a better understanding of the corrosion process.

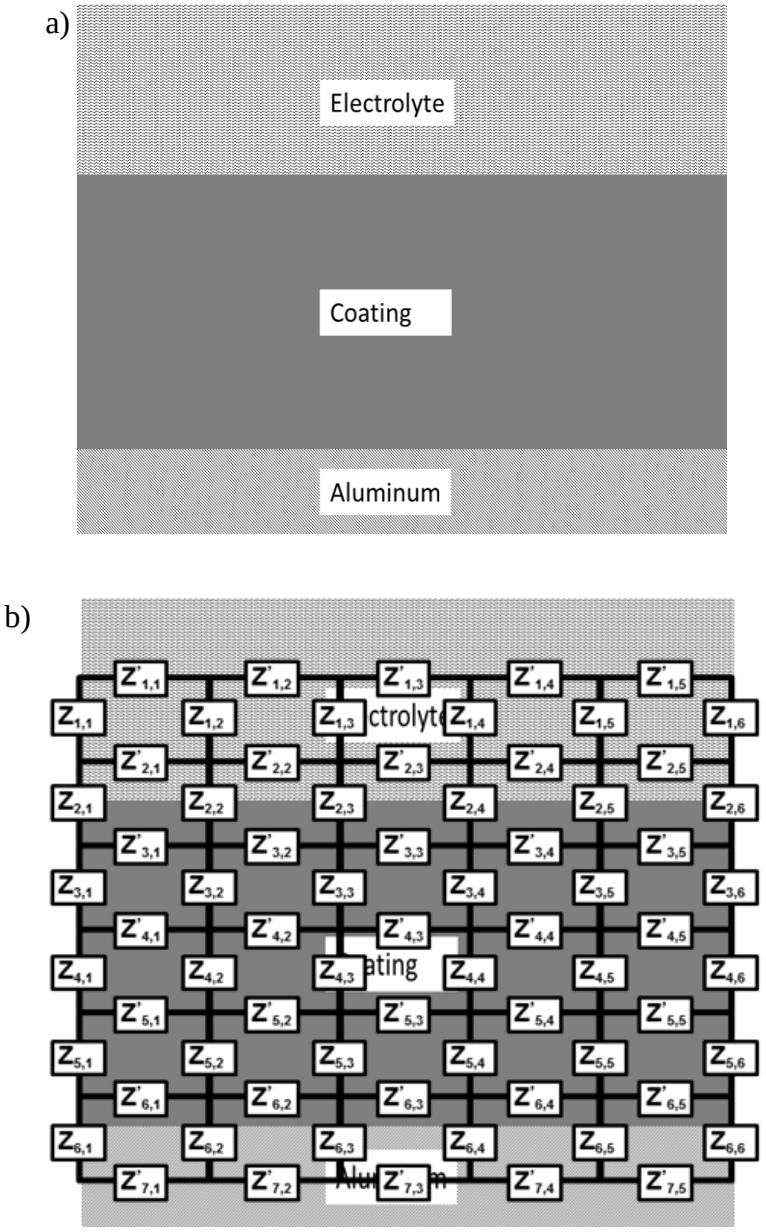

Figure 5.1 a) Lateral profile of experimental system, b) The assigned electro elements distribution in this system

Three cases were studied with the application of 2D transmission line model in this section: 1. initial immersion time (dry coating), 2. Stage I of damage evolution process (coating with water uptake), and 3. Stage II of damage evolution process (activation of electrochemical reaction).

5.1 Application of 2D TLM on dry coating system

In the case of initial immersion time, the tested system profile was indicated as figure 5.2-a, the transmission line model is displayed in the right side of the profile.

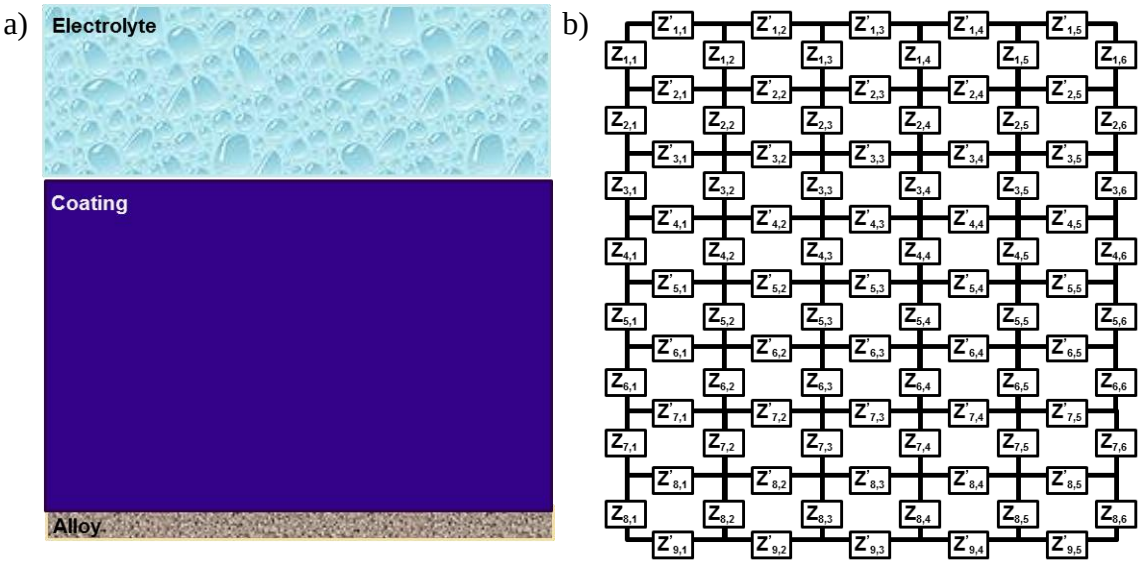

Figure 5.2 a) Lateral profile b) Transmission line representation of hex-chrome free coating(1 mil)/aluminum 2024-T3 system in the initial immersion time

Figure 5.2-b is the detailed elements distribution of the 2D transmission line model in this system. As illustrate by the figure, the Z_1, Z_2 and Z_3 represent the impedance in electrolyte layer which numerically equal to the electrolyte resistance, Z_4 *to*

Z_8 describes the impedance in coating layer, we define a Z_{intact} to represent the impedance of intact coating and the equivalent analogy is showed in figure 5.3.

The mathematically expression for Z_{intact} is as follows:

$$Z_{\text{int}act} = \frac{R_c}{\left(1 + R_c Q_c (\omega i)^n\right)} \tag{4}$$

Where R_c is the resistance of intact coating and constant phase element (*CPE*) is associated to capacitance of intact coating. Z_9 represents the impedance in aluminum substrate which numerically equal to the metal resistance. Similar for the impedance elements (*Z*), each resistance element (*R*) has its own value which describes the physical condition of each layer. The magnitude of each electrochemical element changes over time due to the damage evolution process.

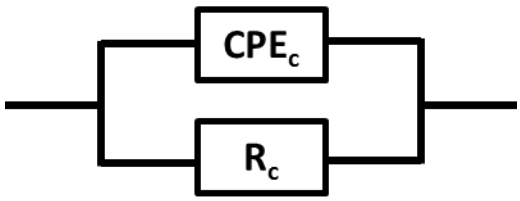

Figure 5.3 Equivalent analogy of impedance representation Z_4-Z_8

A sensitivity analysis is carried out based the on the model described in the previous section, two parameters were investigated in this section: intact coating resistance (R_c) and *CPE* of intact coating

Figure 5.4 shows the impedance spectra while we change the magnitude of R_c. According to the previous work, the coating resistance for dry coating ranges from 10^7 to 10^9 ohm cm^2; so that, we changed R_c from 10^6 to 10^8 ohm cm^2 in the sensitivity analysis.

The magnitude chosen for other parameters analyzed in the following section was carried out under similar consideration. The impedance mode in low frequency range decreased and the phase angle in medium frequency (10^0-10^3 Hz) decreased along with the decreasing of coating resistance. The shape of EIS spectra in Nyquist representation remained the capacitive loop while the radius of the semicircle decrease with the decreasing of coating resistance.

Figure 5.5 is the change of impedance spectra while we change the magnitude of CPE_c. The impedance mode in high frequency decrease and the phase angle in median frequency range increase with the increase of *CPE* magnitude. By increasing the value of CPE_c, the phase angle "peak" moved towards low frequencies and the Nyquist plot shortened in the low frequency zone without showing any other modification to the plots; the meaning of this changes is that the EIS is strongly dependent on these values, R_c will have a stronger effect on the Nyquist plot, and CPE_c in the phase angle plot.

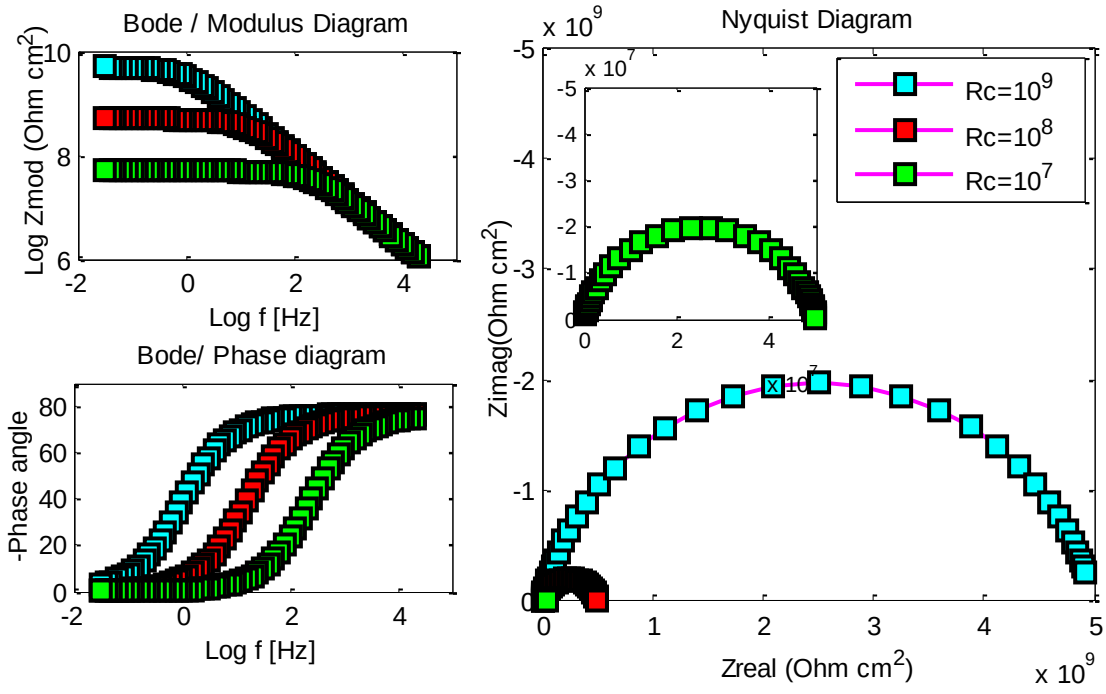

Figure 5.4 Sensitivity analyses for the intact coating resistance

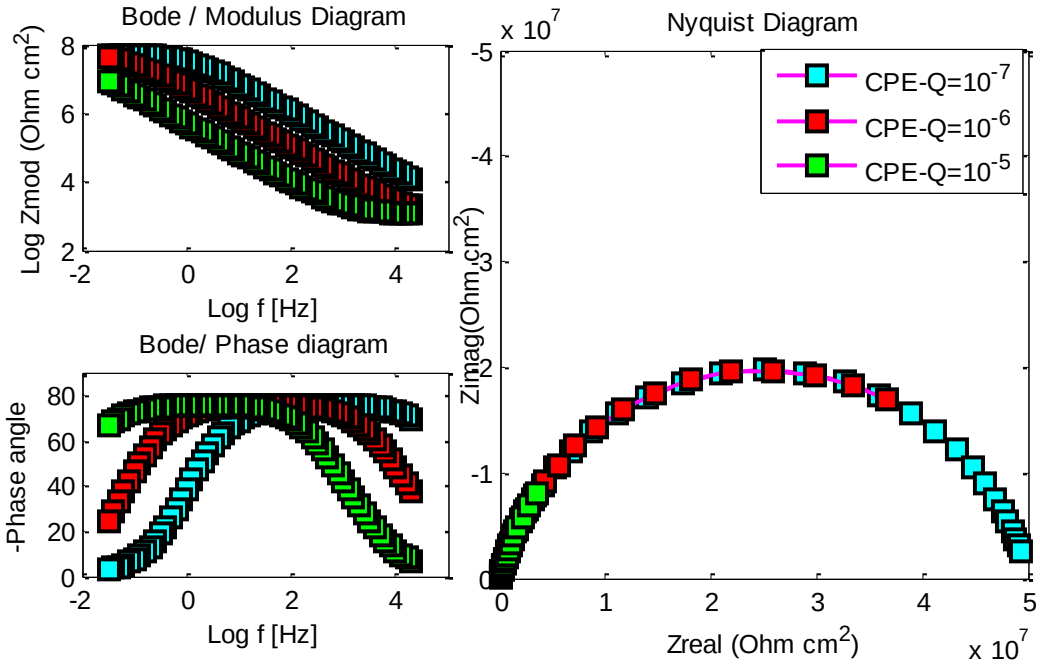

Figure 5.5 Sensitivity analysis for the CPE of intact coating

In the previous section, we analyzed the main parameters that impact the EIS representation. In this section, those parameters were manipulated to obtain a simulated impedance data which had a good agreement with the experimental result in this section. To be more precise, the impedance data simulated from the 2D TLM had an approximate 2% error (evaluated by sum of square error (SSE)) with respect to experimental data.

Figure 5.6 is the comparison between the experimental result and the simulated data in the form of both Nyquist representation and Bode representation. The red round spots were the experimental results the blue rectangle spots were the simulated data.

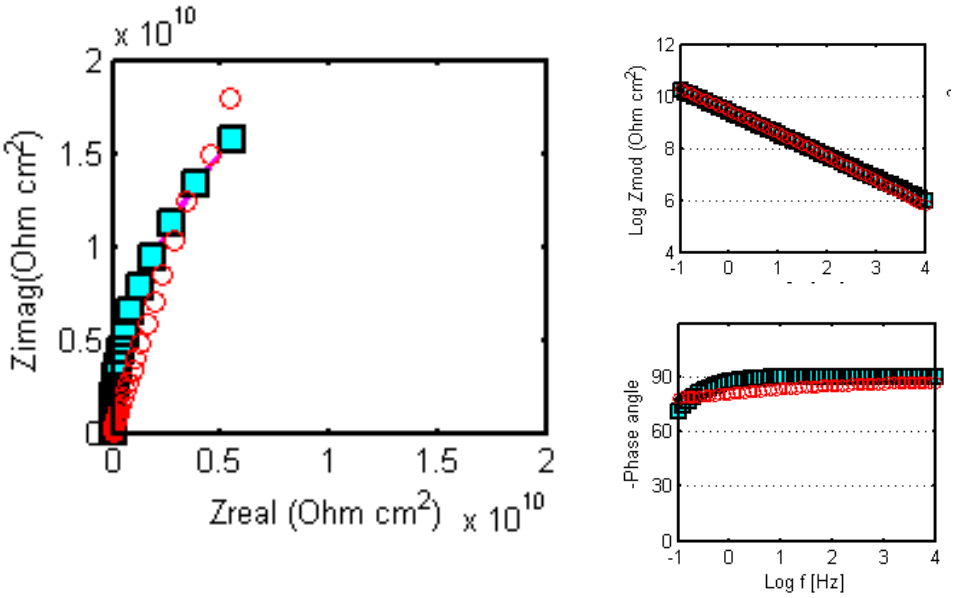

Figure 5.6 Comparisons between the experimental result and the simulated EIS spectra

At the same time, the magnitude of local impedance distribution of each layer for the dry coating was obtained and it is presented in figure 5.7

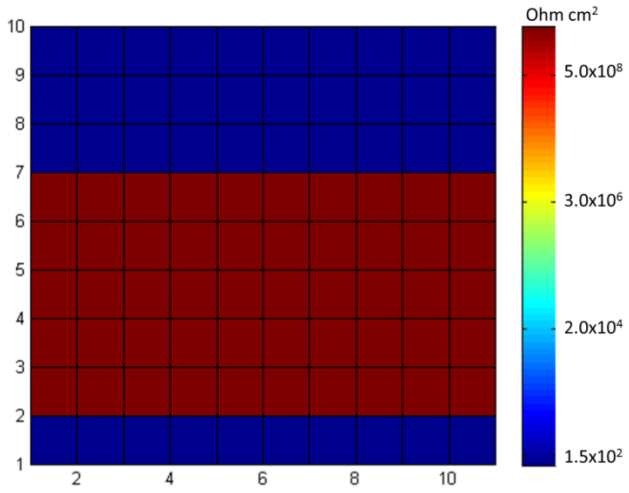

Figure 5.7 The local impedance distribution for dry coating condition

It is straight forward to tell the physical significance of each layer according to Figure 5.7: the blue color which represented the impedance of metal substrate as well as electrolyte has a lower magnitude impedance compare to the red color which denote the coating layer; since the conditions are dry, the profiles shows horizontal lines defining physically the different layers with no alteration due to any chemical or electrochemical reaction.

5.2 Application of 2D transmission line model on stage I of damage evolution process

In this section, we applied the proposed transmission line model on the coating/aluminum system under stage I of damage evolution mechanism, this stage started with the beginning of electrolyte transport through the coating layer and ended when the electrolyte reached the metal substrate and it is the main process in the

coating/metal degradation mechanism. In order to understand the process in detail, we analysis three coating condition in this stage: 1. the initial time of stage I damage evolution process, 2. the early time of stage I damage evolution process, and 3. The later time of stage I damage evolution process.

5.2.1 Equivalent analogy of local impedance elements for coating under initial times of stage I damage evolution process

For the initial electrolyte diffusive process, the degree of electrolyte uptake in the top part of the coating layer is much larger compared to the rest part of coating. Figure 5.8-a is a sketch of the coating system under this condition. Figure 5.8-b is the transmission line model we applied in this case.

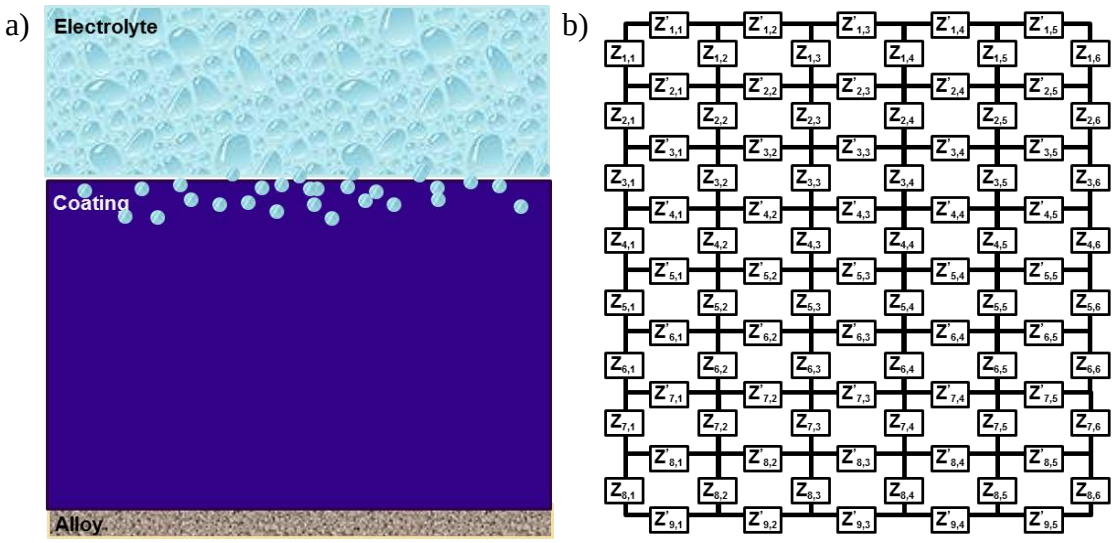

Figure 5.8 a) Lateral profile b) Transmission line representation of hex-chrome free coating(1 mil)/aluminum 2024-T3 system in the initial time of stage I damage evolution process

In this case, Z_1, Z_2 and Z_3 represent the impedance in electrolyte, Z_9 is the impedance of metal which numerally equal to the metal resistance, same as in dry coating case, Z_5-Z_8 describes the impedance of coating area with small degree of electrolyte up take (Z_{intact}) while Z_4 represent the coating part with significant water uptake degree. We defined the coating impedance under partial significant water uptake as $Z_{nonintact}$, and it can be calculated using equation (5)

$$Z_{nonintact} = \frac{Z_{intact} \times Z_{diff}}{\varphi \times Z_{diff} + (1-\varphi) Z_{intact}} \tag{5}$$

In equation (50), φ is the activation parameter ranging from 0 to 1; it describes the proportion of the significant electrolyte diffusion area in the assigned layer. Z_{intact} describes the impedance for portion of coating layer that the electrolyte uptake is negligible and Z_{diff} describes the impedance in the pore where the electrolyte uptake is relative significant.

Figure 5.9 is a sketch of Z_{intact} and $Z_{diffusive}$ in the non-intact coating layer.

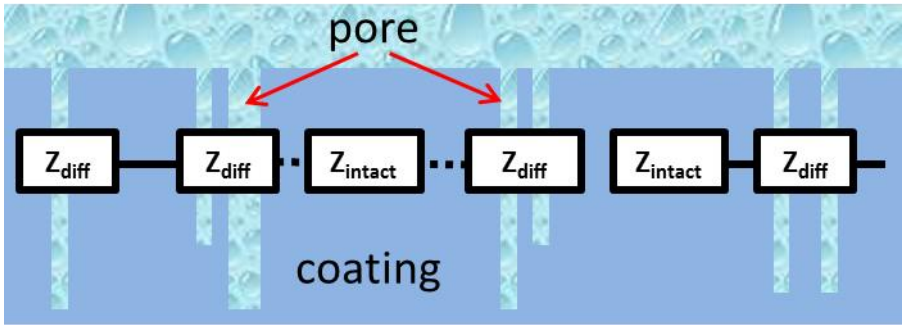

Figure 5.9 Distributions of Z_{intact} and Z_{diff} in the non-intact coating layer

The equivalent analogy accounting for Z_{diff} is shown in figure 5.10. And its mathematically representation is shown in equation 6

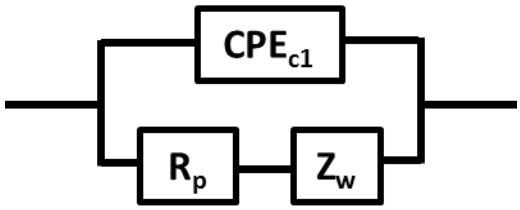

Figure 5.10 Equivalent analogies for $Z_{diffusive}$

$$Z_{diff} = \frac{R_p + Z_w}{\left(1 + \left(R_p + Z_w\right)Q_1(\omega i)^n\right)} \tag{6}$$

Where R_p, the pore resistance, is not only impacted by the physical condition of coating structure but also influenced by the amount of electrolyte accumulated in the pores. Z_w is the impedance of Warburg diffusion element, and it was obtained via equation 7

$$Z_w = \frac{A_w}{\sqrt{\omega}} + \frac{A_w}{j\sqrt{\omega}} \tag{7}$$

In equation 7, A_w is the Warburg coefficient.

A sensitivity analysis based on these parameters in this model were carried out as well, they are: intact coating resistance (R_c), constant phase element of intact coating (CPE_c), Warburg coefficient (A_w), the activation coefficient (φ), pore resistance (R_p), the constant phase element of coating part that has a significant degree of electrolyte uptake (CPE_{c1}).

Figure 5.11 shows the change of EIS spectra for different intact coating resistance (R_c). For coating system under stage I of damage evolution process, the coating resistance obtained from the simple equivalent analogy usually ranges from 10^6 to 10^8 ohm cm^2 , so that, the analysis the EIS behavior for intact coating resistance ranges from 10^6 -10^8 ohm cm^2. According to figure 5.11, the magnitude of total impedance decrease, the phase angle at median frequency (10^0-10^3 Hz) was smaller for the low coating resistance condition. this behavior is consistent with experimental results [45]. Besides, two time constant observed at the Nyquist plot while R_c equals to 10^6ohm cm^2. This EIS behavior suggested the participation of another electrical mechanism (for example, electrochemical reaction in the coating/ substrate interface) in addition of the electrolyte diffusion process in the low intact coating resistance condition.

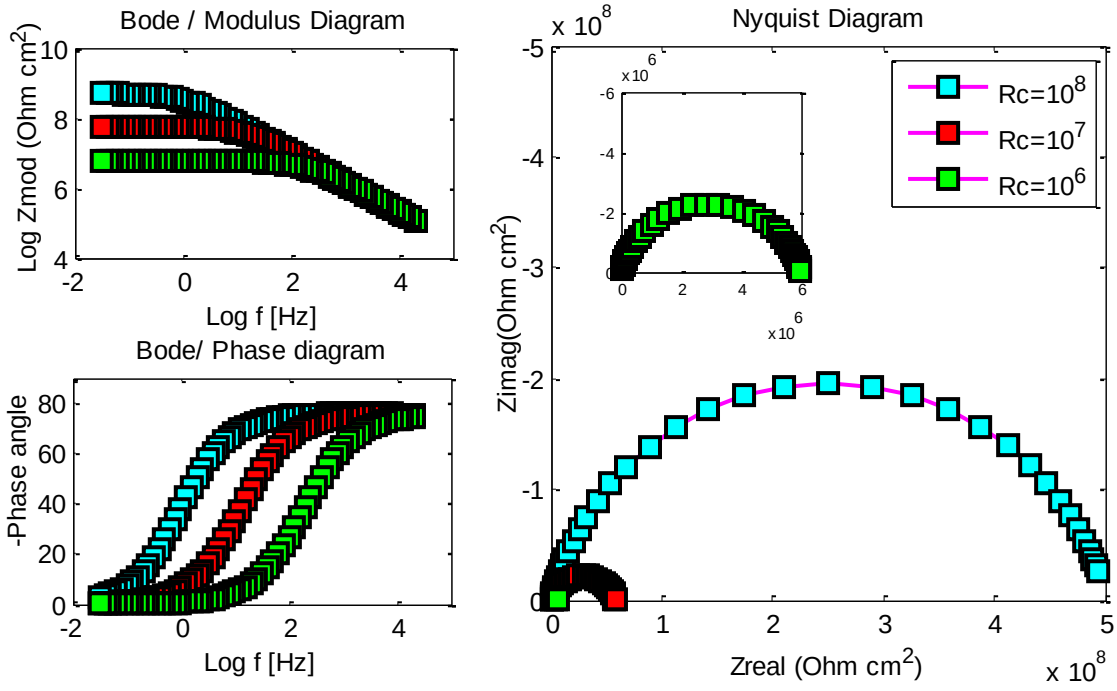

Figure 5.11 Sensitivity analyses for the intact coating resistance (R_c)

Figure 5.12 is the EIS spectra with various CPE_c. The phase angle at median frequency (10^0-10^3Hz) decreases while we increase the magnitude of CPE_c. The magnitude of total impedance at high frequency also decreased. The shape of Nyquist representation for large magnitude CPE_c (10^{-8} and 10^{-7} F s^{-n}) are similar, both of them a semicircle. On the other hand, for CPE_c equals to 10^{-6} F s^{-n}, two overlapped semicircles are observed; this later is due to the ratio of the CPE_{cl} relative to CPE_c, in other words, the presence of CPE_{cl} is detected at low values of CPE_c.

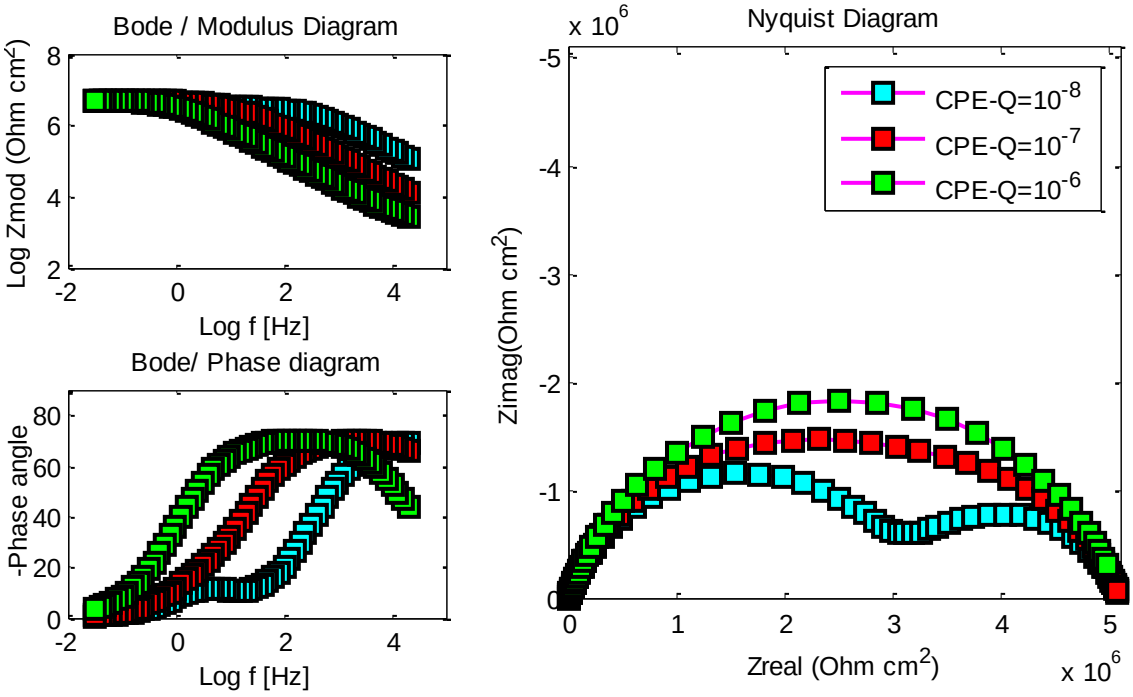

Figure 5.12 Sensitivity analyses for CPE of the intact coating

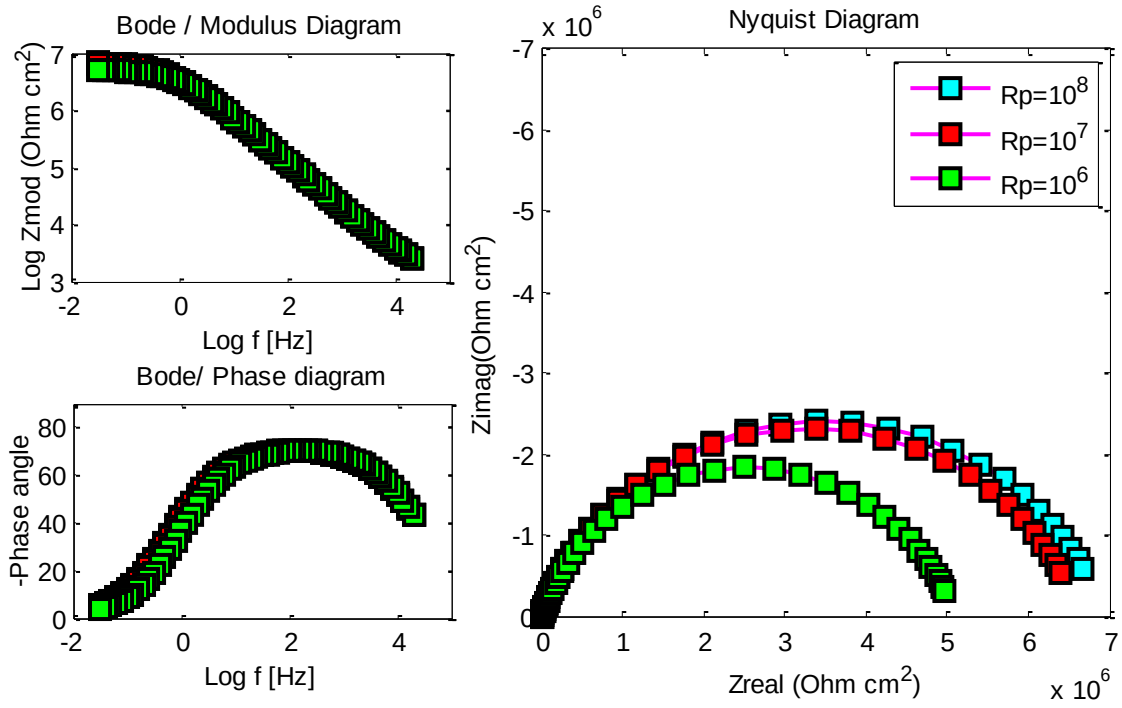

Figure 5.13 Sensitivity analyses for pore resistance *Rp*

Figure 5.13 shows the change of EIS spectra pore resistance (R_p). In this case, the bode plot remains similar while the R_p varies from 10^8 to 10^6 ohm cm^2. The only difference appeared in the Nyquist representation. The radius of semicircle in Nyquist plot slightly decreased while the R_p decrease. The shape of EIS spectra in Nyquist representation did not change while the R_p value decreased. This indicated the R_p in the range of 10^6-10^8 ohm cm^2 does not play a relevant role in EIS behavior.

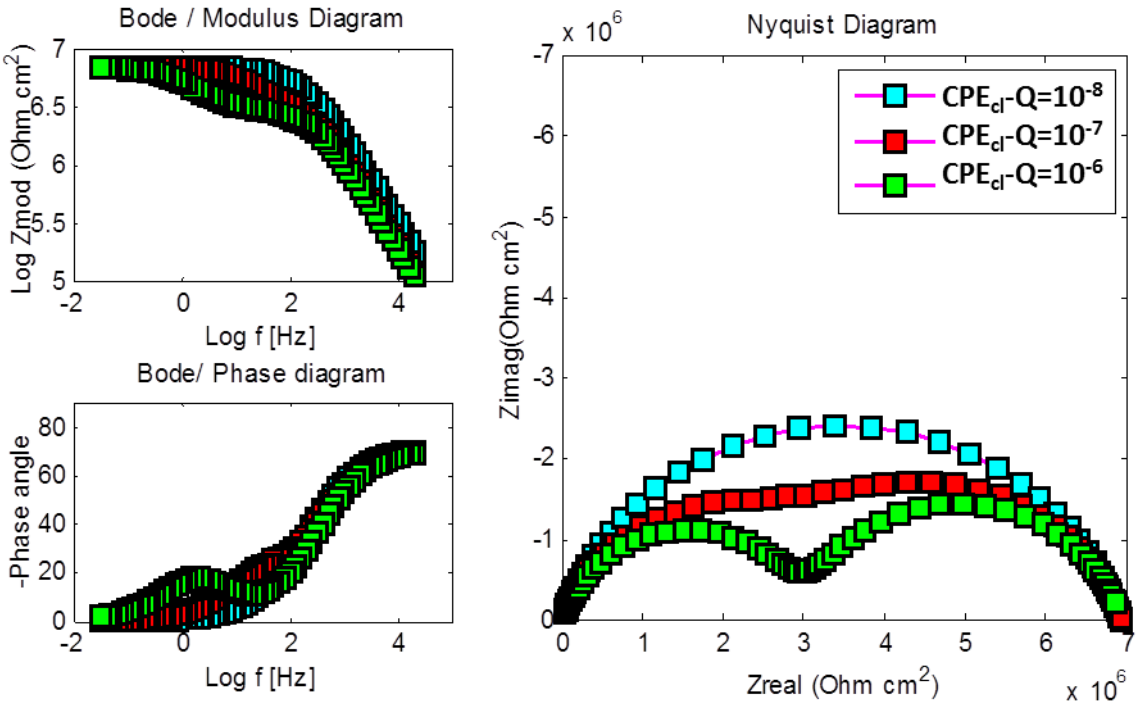

Figure 5.14 Sensitivity analyses for CPE_{cl} of coating porous

Figure 5.14 shows the change of EIS spectra for different (CPE_{c1}). In this case, the bode plot remains similar while the CPE_{c1} varies from 10^{-8} to 10^{-6} F s^{-n}. The only difference appeared in the Nyquist representation. The radius of semicircle in Nyquist decreased while the CPE_{c1} increased. The impact of CPE_{c1} (in the range of 10^{-8} to 10^{-6} F s^{-n}) on the EIS spectra was also small according to the analysis. Two time constants are more defined as long as CPE_{cl} increases, this is also due to the ratio CPE_{cl}/CPE_{c} as it was shown above.

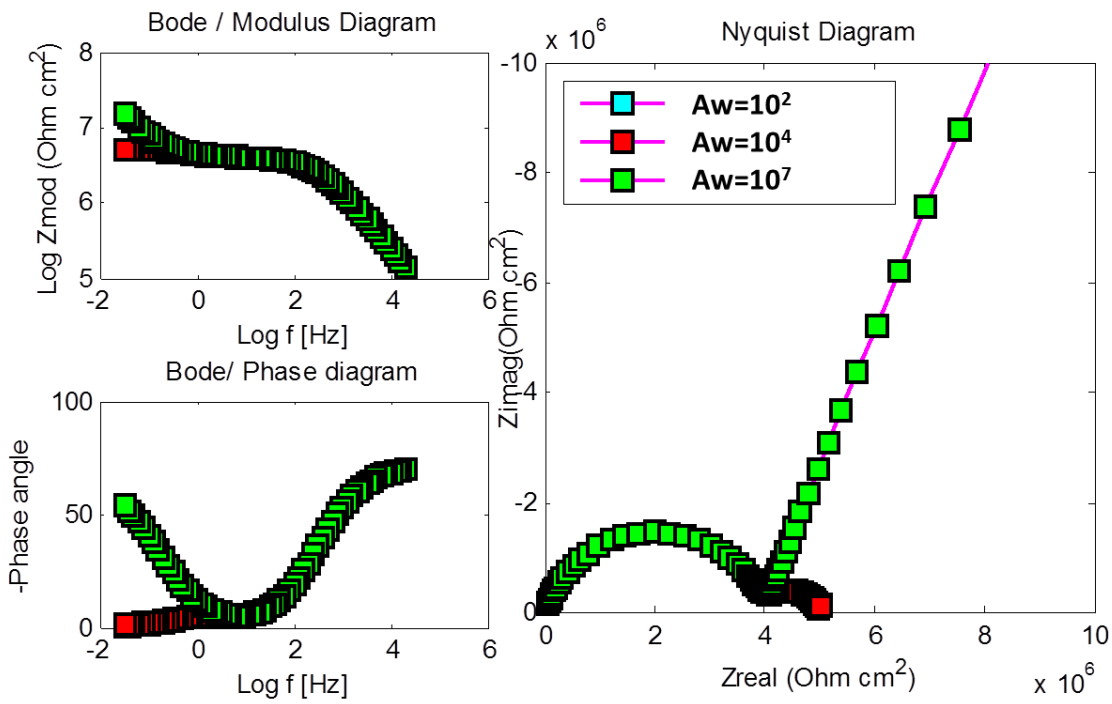

Figure 5.15 Sensitivity analyses for Warburg coefficient

Figure 5.15 is the change of EIS spectra for different Warburg coefficient. According to this figure, two overlapped semicircles are observed on the EIS spectra where Warburg coefficient is around 10^2 and 10^4 ohm $s^{-1/2}$. A typical diffusion behavior appeared while the Warburg coefficient increased to to 10^7 ohm $s^{-1/2}$ as it was expected. The value of the Warburg coefficient relates directly to the resistance of the interface, in this case, the value was sensitive for the selected values of *Rp* and *Rc*.

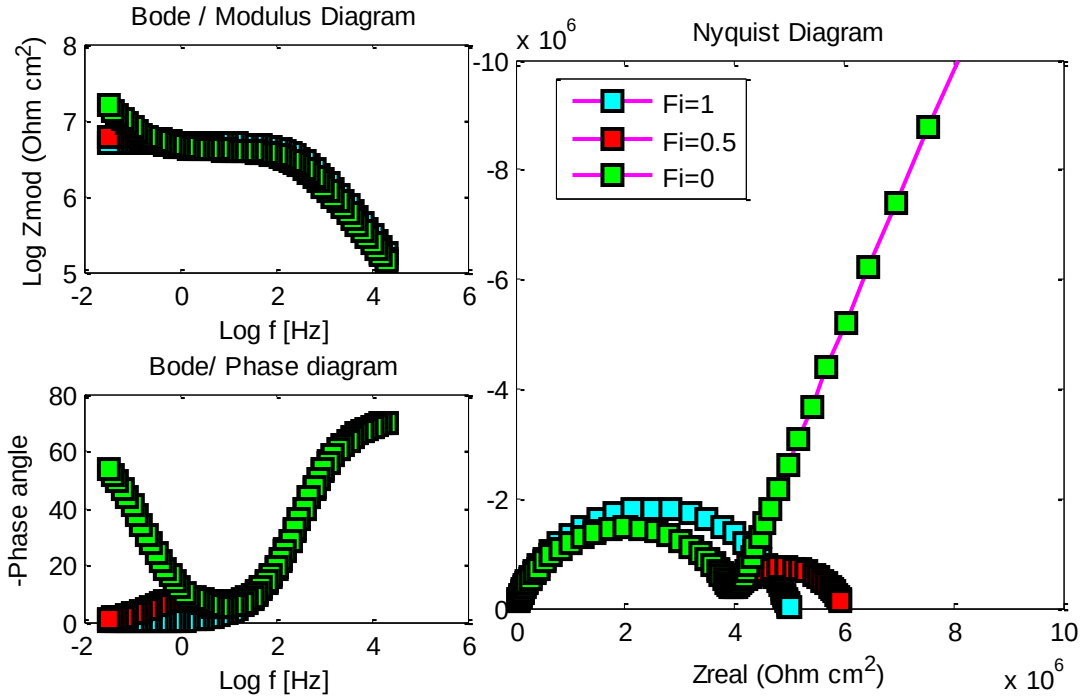

Figure 5.16 Sensitivity analyses for activation parameter

Figure 5.16 shows the change of EIS spectra for different activation coefficient φ. When φ equaled to unity, it indicates no severe diffusion process occurred, the coating layer was intact, only one semicircle appeared in the Nyquist representation, while φ equaled to 0.5, two overlapped semicircle appeared in the Nyquist representation, this means that both processes are taking into account. While φ equaled to zero indicated the electrolyte transport process was significant in whole area, a typical diffusion behavior was observed in both Nyquist and Bode representation.

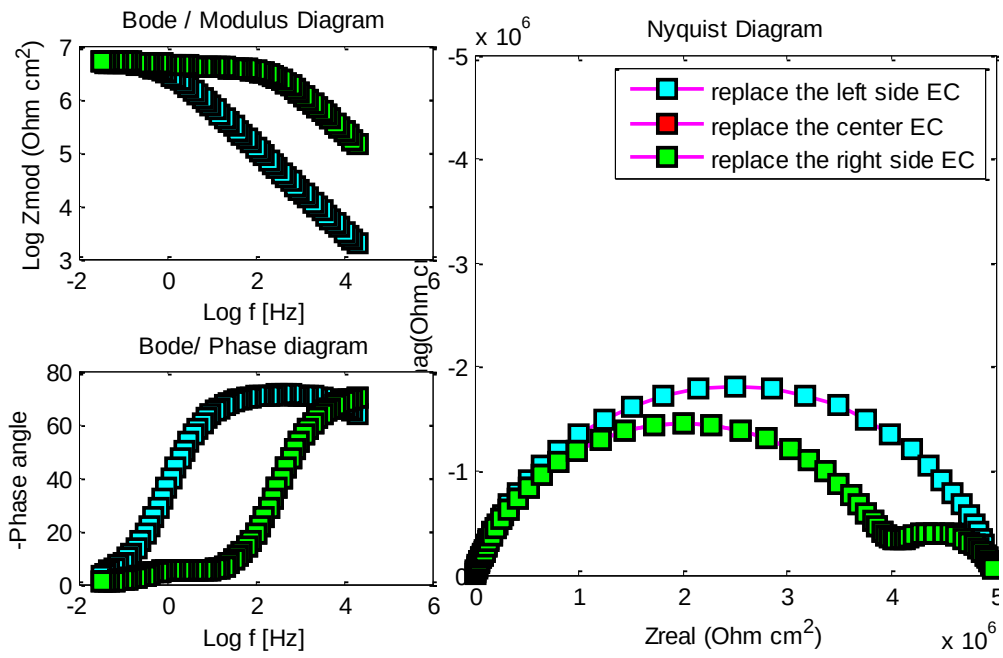

Figure 5.17 Sensitivity analyses for equivalent analogs location

After studied the EIS sensitivity by varying the magnitude of each parameter, the impact of the equivalent elements location was also investigated. The left, center and right sides of Z_{intact} with $Z_{nonintact}$ respectively were replaced; Figure 5.17 is the EIS result. The red data is overlapped with the green data in the figure. Since the center and right side of transmission line model have the same mathematical expression their contribution to the total impedance must be the same. On the contrary, the mathematical expression of the left side equivalent circuit involves the main current according to figure 3.2, so that, any change of equivalent element must impact the EIS spectra as it is observed in Figure 5.17.

By adjusting the parameters investigated in the previous sections, a simulated impedance data which has a good agreement with the experimental results was obtained. To be more precise, the impedance data simulated from the 2D TLM have an

approximate 2% error (evaluated by sum of square error (SSE)) with respect to experimental data. The comparison between the simulated EIS data (blue rectangular spots) and the experimental data (red round spots) is shown in figure 5.18

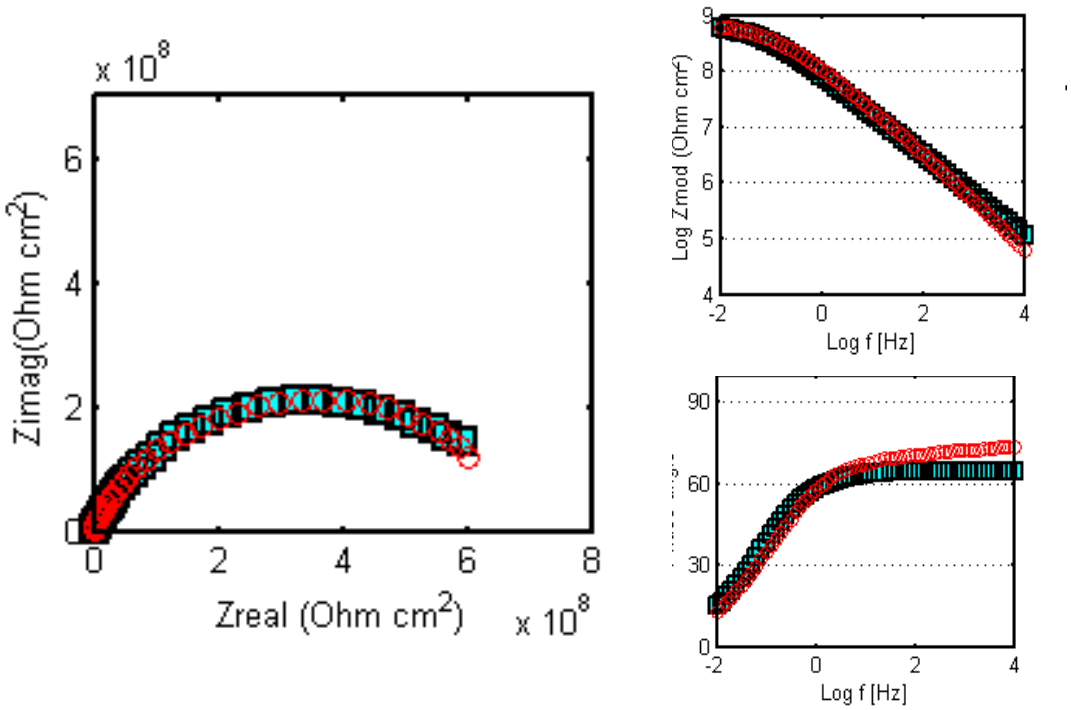

Figure 5.18 Comparisons between the experimental result from day 2 and the simulated EIS spectra

The localized impedance distribution is presented in Figure 5.19. The blue color represents the local impedance in the electrolyte and metal, and its magnitude was about 10^8 ohm cm^2 lower than the impedance in coating layer (indicated as red color in the figure). The impedance of the coating layer which directly contact with electrolyte was relatively lower compare with the rest part of coating. This behavior indicates the water

uptake degree in the top coating layer is higher than the rest part of coating which is something expected due to diffusion conditions.

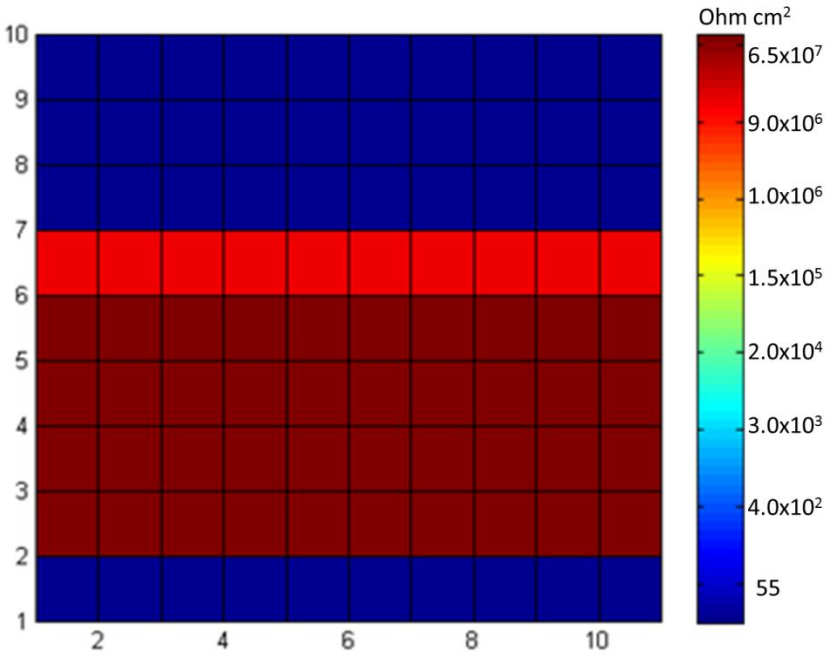

Figure 5.19 The local impedance distribution for coating in initial time of stage I damage evolution mechanism

5.2.2 Equivalent analogy of local impedance elements for coating under early time of stage I damage evolution process

The electrolyte uptake process was a key process in the damage evolution procedure. In order to understand the mechanism of transport process within the coating layer over time in detail, it is mandatory to look at the condition about the early time of

electrolyte uptake process. Figure 5.20-a is the general sketch of the coating profile under this condition. Figure 5.20-b is the transmission line representation for this condition.

In the transmission line, both Z_4 and Z_5 represented the impedance for non-intact coating ($Z_{nonintact}$), which has a mathematically expression same as equation 4. The rest impedance elements remained the same expression as previous. The total impedance was calculated by equation 3 and compared with the experimental EIS data.

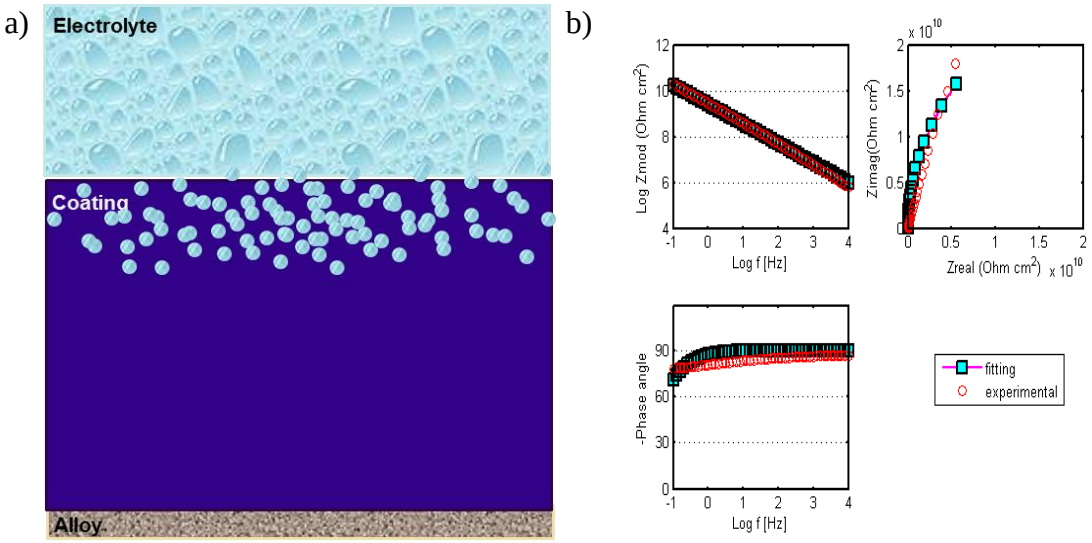

Figure 5.20 a) Lateral profile b) Transmission line representation of hex-chrome free coating (1 mil)/aluminum 2024-T3 system in the early time of stage I of damage evolution process

In Figure 5.21, the red round spots represent the experimental result and the blue rectangle spots is the simulated data. The simulated data has a good agreement with the experimental result. The simulated local impedance distribution was also presented in figure 5.22, it intuitively shows the area with relatively low impedance in the coating layer was increased compare with the early time.

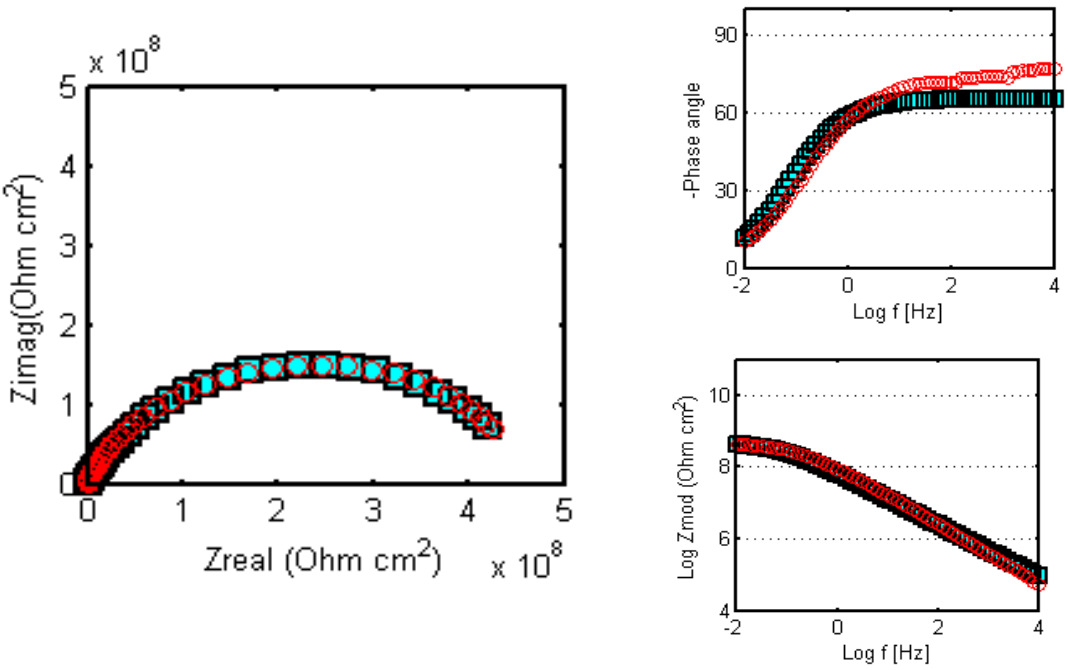

Figure 5.21 Comparisons between the experimental result from day 3and the simulated EIS spectra

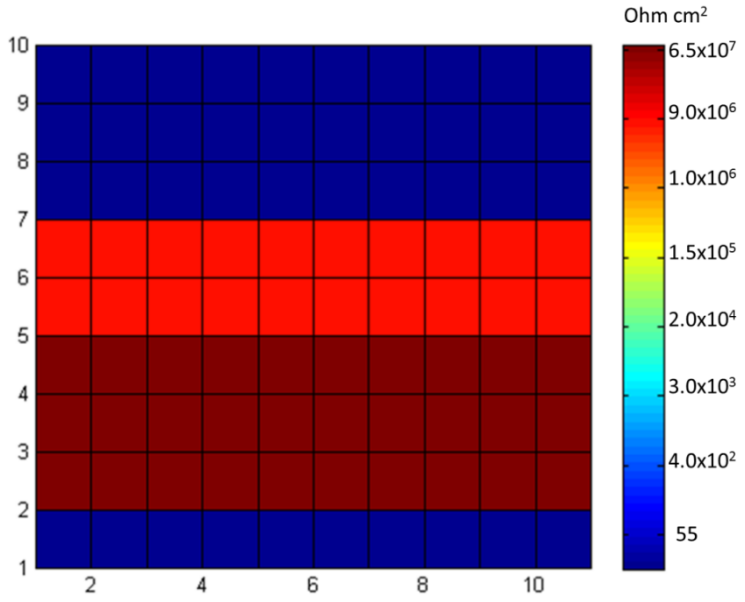

Figure 5.22 The local impedance distribution for coating in early time of stage I damage evolution mechanism

5.2.3 Equivalent analogy of local impedance elements for coating under later time of stage I damage evolution process

The third case we studied in this section is the later time of stage I damage evolution process. In this case, we assumed the electrolyte was almost diffusive through the coating layer, and the electrochemical reaction was about to be activated. Figure 5.23-a is the profile sketch of coating/aluminum system. Figure 5.23-b is a transmission line representation for this stage.

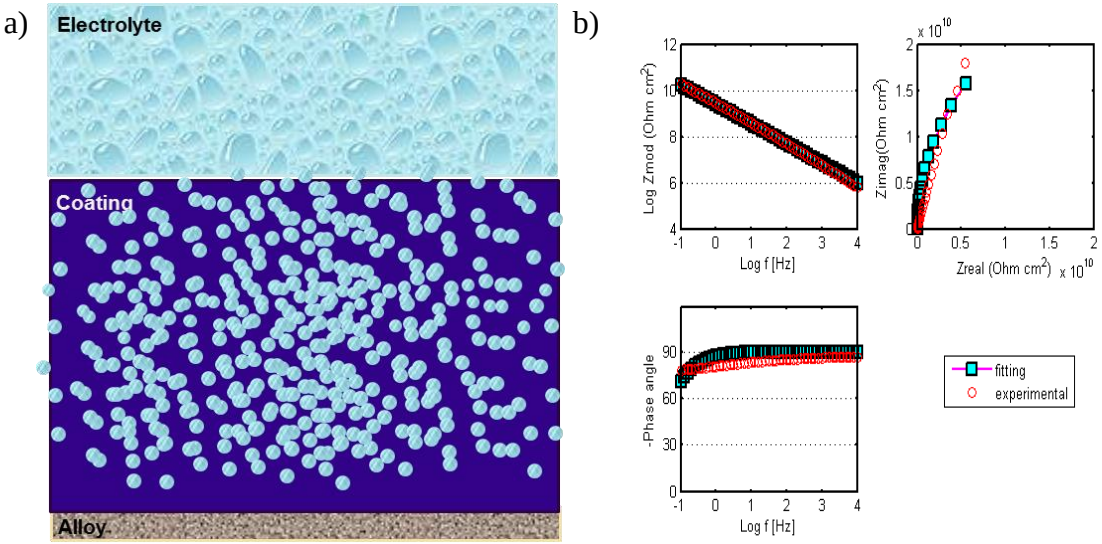

Figure 5.23 a) Lateral profile b) Transmission line representation of hex-chrome free coating (1 mil)/aluminum 2024-T3 system in the later time of stage I of damage evolution process

In this transmission line, Z_4 to Z_7 represent the impedance for coating that already had the electrolyte diffusion ($Z_{nonintact}$), the mathematical expression is show in equation 4. The other impedance elements remain in the same expression as before.

The total impedance was calculated by equation 3 and compared with the experimental EIS data. In Figure 5.24, the red round spots are the experimental result and the blue rectangle spots are the simulated data.

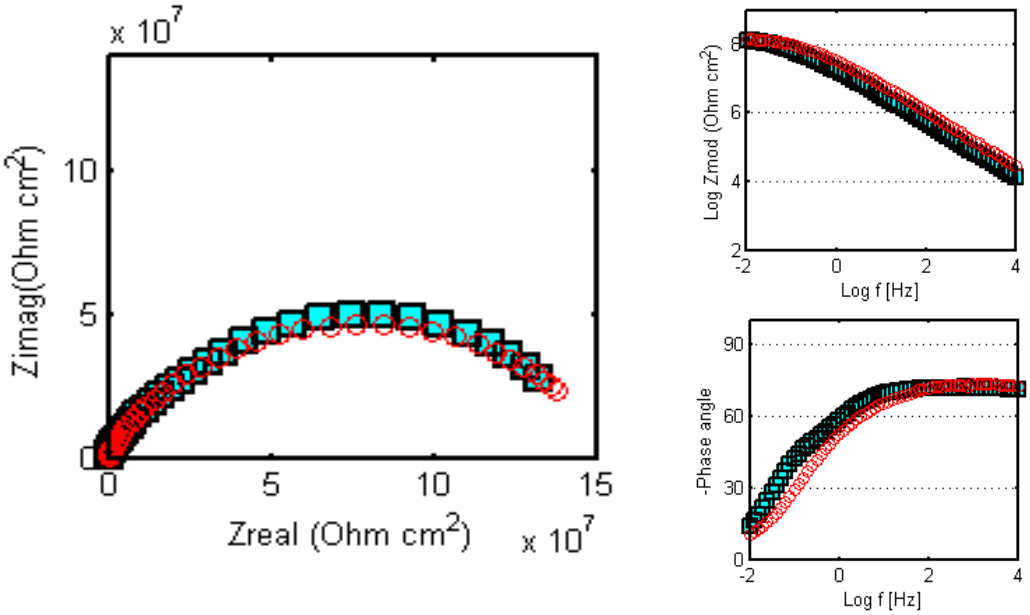

Figure 5.24 Comparisons between the experimental result from 25 days and the simulated EIS spectra

The localized impedance distribution is also presented in figure 5.25; in this figure, the impedance of the majority coating part was lower than the coating impedance in the previous two conditions. It indicated the water uptake degree was large and a large amount of electrolyte was about to reach the metal substrate.

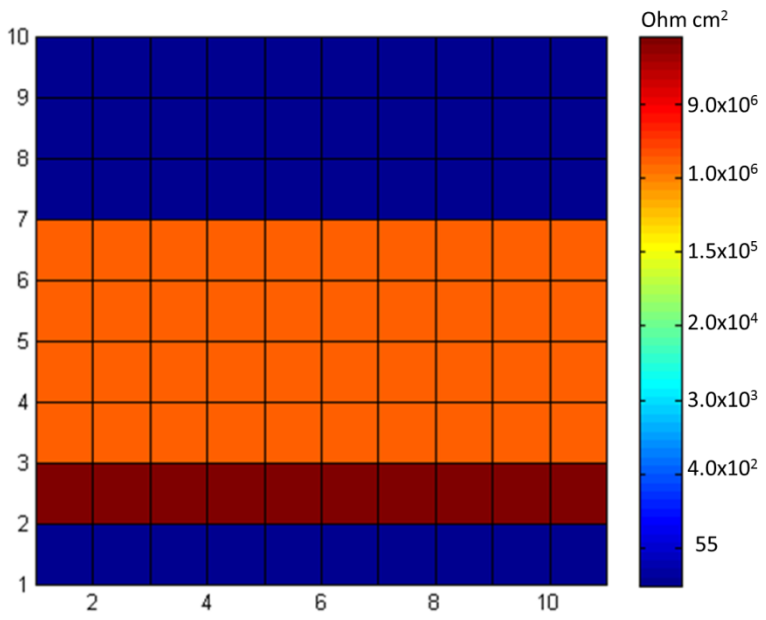

Figure 5.25 The local impedance distribution for coating in later time of stage I damage evolution mechanism

5.3 Application of 2D TLM on coating/aluminum system under stage II of damage evolution process

The third case we studied in this work is the electrochemical reaction activation stage; in this stage, we assume plenty electrolyte penetrated through the coating layer and reached the metal substrate, the electrochemical reaction occurred at this point.

Figure 5.26-a is the sketch of this case. As indicated in the figure, a small amount of corrosion products appeared underneath the coating layer due to the electrochemical reaction. Figure 5.26-b is the transmission line model applied in this case.

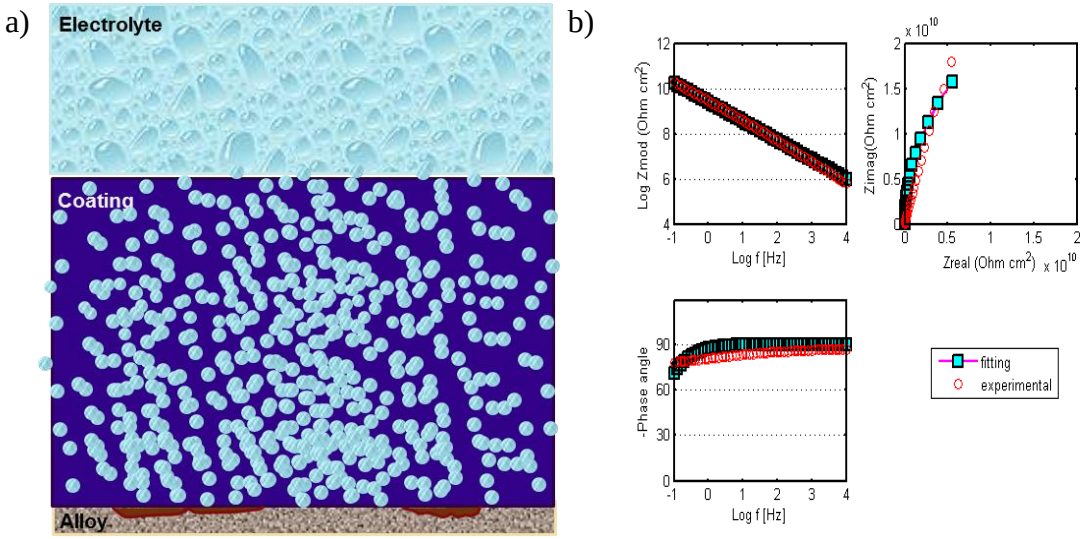

Figure 5.26 a) Lateral profile b) Transmission line representation of hex-chrome free coating(1 mil)/aluminum 2024-T3 system in II of damage evolution process

For this transmission line, Z_1-Z_3 describe the impedance in the electrolyte, which is numerically equal to the electrolyte resistance, Z_4-Z_8 describe the impedance in the coating layer, which is represented by $Z_{nonintact}$ and its mathematical expression is in equation 4. Z_9 represents the impedance for metal substrate with small amount of oxidation products. The equivalent circuits used in this section are the same as in the previous sections.

We first fitted the simulated EIS impedance with the experimental data from 45 days immersion in figure 5.27. We obtained the values for each parameter involved in the transmission line model. Those parameters will be discussed it in the section 5.4

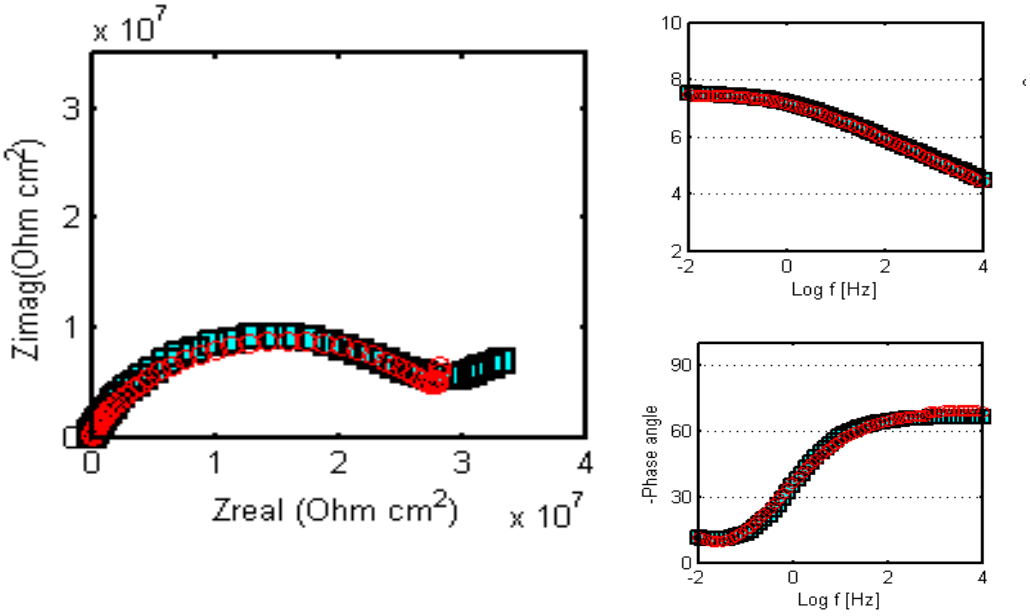

Figure 5.27 Comparisons between the experimental result from 45 days and the simulated EIS spectra

The simulated impedance distribution is quite similar to that one of figure 5.7 with the only difference on the impedance magnitude. The experimental data from 60 days immersion time has the similar Nyquist representation as the one from day 45. In order to understand the difference between them and obtain the detailed degradation mechanism, we also applied the 2D transmission line model on the experimental data from day 45. Figure 5.28 is the comparison between the experimental results (red round spot) and the simulated results (green rectangular spots). The parameters obtained from the optimization fitting will be discussed in section 5.4

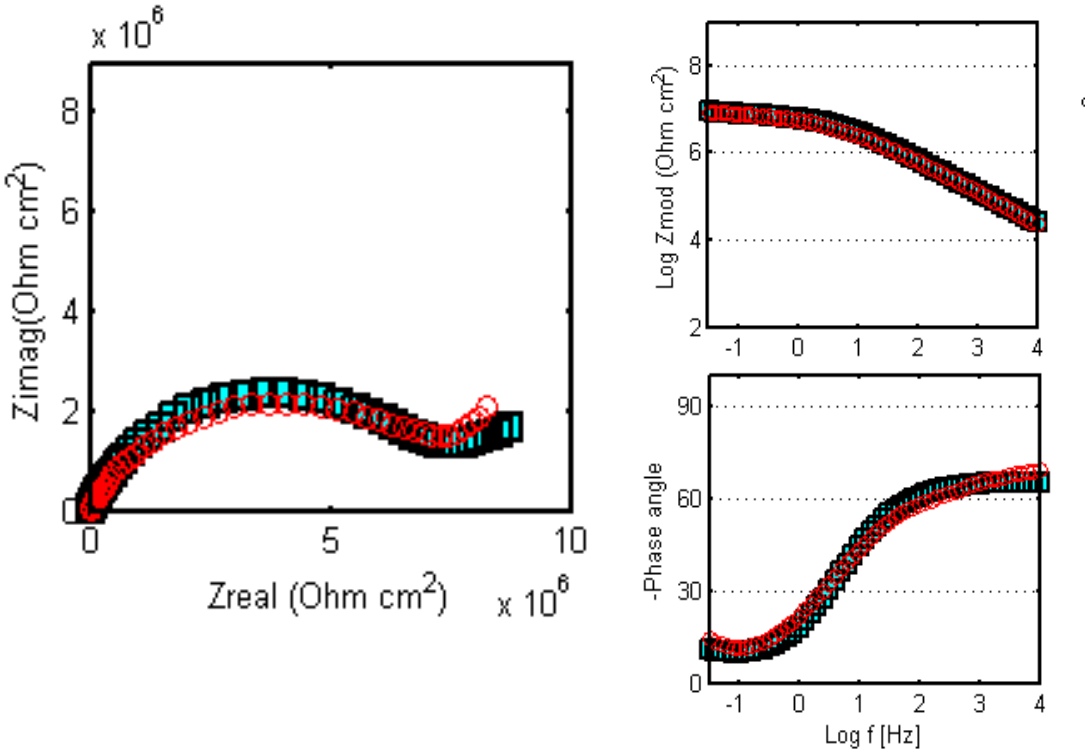

Figure 5.28 Comparisons between the experimental result from 60 days and the simulated EIS spectra

5.4 Discussion

In the previous sections, we studied three damage evolution cases based on the hex-chrome free coating (1mil)/aluminum 2024-T3 system immersed in 3.5% wt NaCl pH 4.0 electrolyte. These three cases are: 1) initial immersion time, 2) stage I of damage evolution process, and 3) Stage II of damage evolution process. The proposed 2D transmission line model is applied on all the cases to help us understand the detailed degradation mechanism better.

In case I, the mentioned coating/aluminum system is under initial immersion time, the electrolyte diffusion process within the coating layer is negligible at this time. As showed in the figure 5.7, the magnitude of the impedance for intact coating layer is much larger compare to the impedance in electrolyte and aluminum. The intact coating resistance (R_c) obtained from the application of 2-D TLM is 1×10^{10}ohm cm^2. Coating is considered under dry condition and served as an isolated layer.

The second case we studied is the stage I of damage evolution process. In this stage, the main process that affected degradation rate is the electrolyte diffusion process within coating layer. According to the experimental result, this stage lasts until 25 days for hex-chrome free coating (1mil)/aluminum 2024-T3 system in pH4.0 electrolyte. In order to see the evolution of coating condition with time in this stage as well as obtaining a detailed understanding of the electrolyte transport process within the coating layer, we investigated three conditions under this stage with the help of a 2-D TLM. The three conditions are: 1. initial time of stage I; 2. early time of stage I; and 3. later time of stage I. The experimental data from day 2, day 3 and day 25 were used for the study of correspondent condition. Two types of coating resistance were obtained from the 2-D TLM: the resistance for intact coating (R_c) and the pore resistance (R_p). The first variable (R_c) describes the general performance of intact coating; the latter variable (R_p) reflected the combination impact of coating degradation and electrolyte accumulation.

For the initial time of stage I damage evolution process, as showed in figure 5.19, the impedance magnitude of the coating layer decreased compare with the initial immersion time, especially for the top surface of coating layer on day 2. This indicated the effect of water uptake process becoming important in stage I of damage evolution

mechanism. In addition, the top part of coating possessed a larger water uptake degree compare to the rest part of the coating layer. This is because the top surface has a direct contact with electrolyte layer. The magnitude of intact coating resistance (R_c) obtained from the 2-D TLM is around 1.5×10^8 ohm cm^2 and the magnitude of pore resistance (R_p) is around 1.2×10^8 ohm cm^2. The small difference between R_c and R_p suggested that only a small amount of electrolyte accumulated in the top part of the coating layer and did not considerably affected the magnitude of the coating resistance.

In the early stage of damage evolution process, figure 5.22 intuitively shows the a coating area with a higher electrolyte uptake. The resistance for intact coating remains 1.5×10^8 ohm cm^2 while the magnitude of pore resistance (R_p) decreased to 5.2×10^6 ohm cm^2. The big change in the magnitude of R_p (almost two orders of magnitude) indicated a higher amount of electrolyte accumulated in the top part of coating layer.

In the later time of stage I damage evolution mechanism, most part of the coating was penetrated with electrolyte. The electrochemical reaction in the coating/substrate interface is about to occur under this instance. The local impedance shown in figure 5.25 strongly supported this idea. In addition, the resistance for intact coating (R_c) decreased to 1.3×10^8 ohm cm^2 while the magnitude of pore resistance (R_p) further decrease to 1.2×10^6 ohm cm^2. The latter indicated a larger amount of electrolyte accumulation per area in the coating part that was penetrated.

The third case we studied is the stage II of damage evolution mechanism. After plenty electrolyte penetrated through the coating layer and reached the aluminum substrate, the electrochemical reaction was activated. This is an indication of the system

transiting from stage I to stage II. In this stage, the concentration of active species in the coating/aluminum interface was lowered due to consumption from the electrochemical reactions. The diffusion process is the main process that controls the degradation rate and the impedance representation (Nyquist plot) reflected this influence. The color representation of local impedance distribution will be similar as the figure 5.7 but the magnitude would be smaller. By optimizing the fitting results between the experimental data from day 45 and the simulated data, R_c is obtained; the magnitude of intact coating resistance (R_c) obtained from the model is around 1.2×10^7 ohm cm^2 which is one magnitude smaller than the R_c from day 25. The magnitude of pore resistance (R_p) is around 1.0×10^6 ohm cm^2 which is similar to the impedance magnitude at final time in stage I. This suggested small degradation occurred in coating layer compare to final time of stage I damage evolution, nevertheless the amount of electrolyte accumulated within the coating layer remained the same on day 45. Another fitting process carried out on the experimental data from day 60 showed that the magnitude of intact coating resistance (R_c) decrease to 2.0×10^6 ohm cm^2, and the resistance of coating layer with high water uptake process remains 1.0×10^6 ohm cm^2. This suggested the coating was further degraded while the amount of electrolyte remained in the coating was the same.

Figure 5.29-a is the R_c over time and figure 5.29-b is the R_p over time. According to the figure, we can see the coating degradation as well as the electrolyte accumulating process in coating over time.

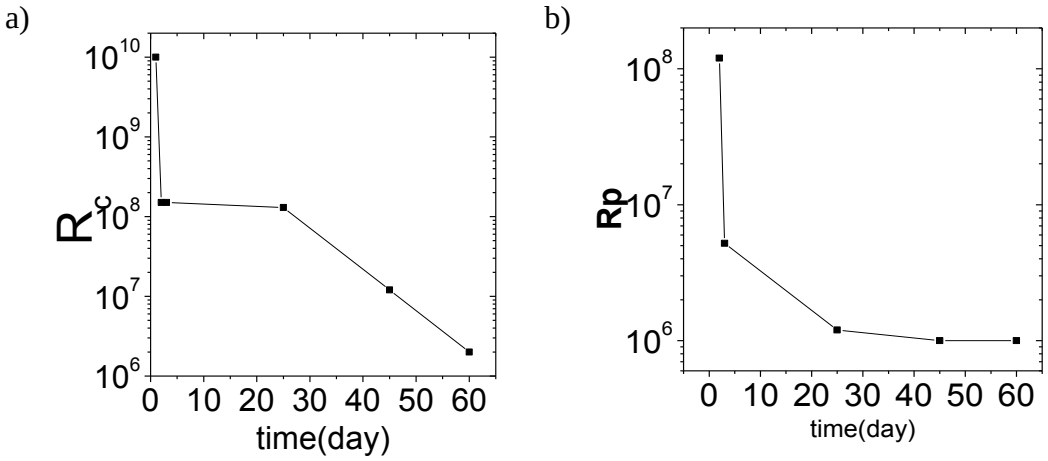

Figure 5.29 a) Resistance of intact coating (R_c); b) Pore resistance (R_p) over time

CHAPTER VI

CONCLUSION

In this work, we designed an environmental friendly hex-chrome free coating/aluminum system. In order to understand the degradation mechanism of this coating system better, we investigated the corrosion behavior of this coating/steel system under constant immersion environment. Three experimental variables were investigated in this work; they are electrolyte pH, top coat thickness and the metal substrate.

By interpreting the EIS results for each case, we concluded

1. The 3.5 wt% NaCl, pH 4.0 electrolytes simulated the most corrosive environment compared to pH 7.0 and pH 10.0 electrolyte. under 160 days of immersion in pH 4.0 electrolyte, the coating/aluminum system was in stage II of damage evolution mechanism, while the system immersed in the other two pH electrolyte were still in the stage I of damage evolution mechanism.
2. According to the EIS representation from the sample immersed in the most corrosive environment, we conclude the coating is dry and intact in the initial immersion time, electrolyte transport process and electrochemical reaction process occurred after certain time, an condensed oxide products layer is formed in the coating substrate interface around 100 days, diffusion process within the oxide layer is the predominant process that impact the corrosion rate at that time.

3. Change the top coating thickness from 0.025mm to 0.075mm will not affect the corrosion mechanism much, the system with thicker top coating has only a slightly better performance compare to the thinner ones according to the impedance representation.
4. Two metal substrates are used in this work; the substrate will not affect the early stages of damage evolution process. However, in stage II of damage evolution process, we found the aluminum 7075-T6 is more susceptible to corrode compare to the aluminum 2024-T3.

With the help of the previous work, we introduced the damage evolution concept in this work. General speaking, the damage evolution mechanism include four steps: I) electrolyte transfer process within coating layer; II) The initialization of electrochemical reaction in the coating/metal interface, the electrochemical products started to form under neater coating layer; III) The charge transfer dominates process; the electrochemical products propagated and degradation and delamination occurred on coating; and IV) coating failure, electrolyte directly contact with substrate, metal experience several loss.

In order to study the detailed damage evolution mechanism base on the Hex-Chrome free polyurethane coating/aluminum system, we developed a 2-D transmission line model based on Kirchhoff's laws.

Three damage evolution cases were investigated alone with the application of 2-D TLM. The model was firstly verified by the EIS spectra obtained from the experimental result. A further application of this 2D TLM revealed the local impedance distribution

along the profile of coating/aluminum system. By studying the impedance distribution, we conclude:

1. The main process in the coating/aluminum system immersion test is electrolyte uptake process in the coating layer and the electrochemical reaction beneath coating layer.
2. In the initial time of immersion, the electrolyte uptake degree is much higher for the top area which is directly in contact with the electrolyte compare to the rest part of coating. besides, the electrolyte uptake degree is increasing over time in the following two ways according to the impedance magnitude: the electrolyte penetrated more area with time and the amount of electrolyte accumulated per area was increasing as well.
3. An electrochemical reaction was activated on day 45 for the tested sample system, the coating resistance obtained from the 2-D TLM was decreasing in magnitude compare to previous days (day 25) which indicates that the coating was degrading over time. The pore resistance (R_p) did not change much, which, suggested that the electrolyte amount accumulated in the coating layer did not have important changes as well. The similar trend was observed in the EIS data from day 45 of immersion.

BIBLIOGRAPHY

[1] R.. Parkhill, E.. Knobbe, M.. Donley, Application and evaluation of environmentally compliant spray-coated ormosil films as corrosion resistant treatments for aluminum 2024-T3, Prog. Org. Coatings. 41 (2001) 261–265.

[2] D. Wang, Y. Ni, Q. Huo, D.E. Tallman, Self-assembled monolayer and multilayer thin films on aluminum 2024-T3 substrates and their corrosion resistance study, Thin Solid Films. 471 (2005) 177–185.

[3] N. Voevodin, N. Grebasch, W. Soto, L. Kasten, J. Grant, F. Arnold, et al., An organically modified zirconate film as a corrosion-resistant treatment for aluminum 2024-T3, Prog. Org. Coatings. 41 (2001) 287–293.

[4] V. Cicek, environmentally friendly corrosion inhibition of sol-gel coated al 2024-t3 alloy, (n.d.).

[5] P. Pedeferri, Cathodic protection, 10 (1996) 391–402.

[6] F. Mansfeld, Electrochemical impedance spectroscopy (EIS) as a new tool for investigating methods of corrosion protection, Electrochim. Acta. 35 (1990) 1533–1544.

[7] W. Funke, Polymer Matetials for Corrosion Control, 1986.

[8] Y. Joshua Du, M. Damron, G. Tang, H. Zheng, C.-J. Chu, J.H. Osborne, Inorganic/organic hybrid coatings for aircraft aluminum alloy substrates, Prog. Org. Coatings. 41 (2001) 226–232.

[9] R.L. Twite, G.P. Bierwagen, Review of alternatives to chromate for corrosion protection of aluminum aerospace alloys, Prog. Org. Coatings. 33 (1998) 91–100.

[10] J. Zhao, Corrosion Protection of Untreated AA-2024-T3 in Chloride Solution by a Chromate Conversion Coating Monitored with Raman Spectroscopy, J. Electrochem. Soc. 145 (1998) 2258.

[11] H. Umehara, M. Takaya, S. Terauchi, Chrome-free surface treatments for magnesium alloy, Surf. Coatings Technol. 169-170 (2003) 666–669.

[12] T.L. Metroke, R.L. Parkhill, E.T. Knobbe, Passivation of metal alloys using sol–gel-derived materials — a review, Prog. Org. Coatings. 41 (2001) 233–238.

[13] P.R. Chalker, S.J. Bull, D.S. Rickerby, A review of the methods for the evaluation of coating-substrate adhesion, Mater. Sci. Eng. A. 140 (1991) 583–592.

[14] X.H. Chen, C.S. Chen, H.N. Xiao, F.Q. Cheng, G. Zhang, G.J. Yi, Corrosion behavior of carbon nanotubes–Ni composite coating, Surf. Coatings Technol. 191 (2005) 351–356.

[15] M.A. Nicholls, T. Do, P.R. Norton, G.M. Bancroft, M. Kasrai, Chemical and mechanical properties of ZDDP antiwear films on steel and thermal spray coatings studied by XANES spectroscopy and nanoindentation techniques, 15 (2003) 241–248.

[16] C.Y. Tang, Y.-N. Kwon, J.O. Leckie, Effect of membrane chemistry and coating layer on physiochemical properties of thin film composite polyamide RO and NF membranes, Desalination. 242 (2009) 149–167.

[17] J.N. Murray, Electrochemical test methods for evaluating organic coatings on metals: an update. Part II: single test parameter measurements, Prog. Org. Coatings. 31 (1997) 255–264.

[18] Ulick R. Evans, The corrosion and Oxidation of Metals, Hodder Arnold, 1960.

[19] F.S.B. R., Mechanism of cathodic protectioin of zinc-rich points by electrochemcial impedance spectrospy i Galvanic stage, J. Coat. Technol. 61 (1989) 63–69.

[20] S.R. Yeomans, Performance of Black , Galvanized , and Epoxy-Coated Reinforcing Steels in Chloride-Contaminated Concrete 8, (1994).

[21] H.D. Cooley, Air Force Institute of Technology, (n.d.).

[22] D. Kaushik, M.N. Alias, R. Brown, An Impedance Study of a Carbon Fiber/Vinyl Ester Composite, Corrosion. 47 (1991) 859–867.

[23] L.M.Callow, Corrosion Monitoring using Polarisation Resistance Measurement: II Source of error, Br. Corros. J. 11 (1976) 132–139.

[24] J.N. Murray, Electrochemical test methods for evaluating organic coatings on metals: an update. Part III: Multiple test parameter measurements, Prog. Org. Coatings. 31 (1997) 375–391.

[25] H. Xiao, Evaluation of Coating Degradation with Electrochemical Impedance Spectroscopy and Electrochemical Noise Analysis, J. Electrochem. Soc. 141 (1994) 2332.

[26] G.B. Xianping Wang, Dennis Tallman, Use of Electrochemical Noise Methods for Predicting Early-stage Corrosion and Monitoring Coating Degradation During Atmospheric Exposure, Electrochem. Soc. (1999) 2761.

[27] M.M. Musiani, Characterization of Electroactive Polymer Layers by Electrochemical Impedance Spectroscopy (eis), 35 (1990) 1665–1670.

[28] VersaSCAN Electrochemical Scanning Base System, 2012.

[29] H. Castaneda, J. Alamilla, R. Perez, Life Prediction Estimation of an Underground Pipeline Using Alternate Current Impedance and Reliability Analysis, Corrosion. 60 (2004) 429–436.

[30] A. Amirudin, D. Thierry, IN ORGANIC Application of electrochemical impedance spectroscopy to study the degradation of polymer-coated metals, 9440 (1995).

[31] J.R. Park, D.D. Macdonald, Impedance studies of the growth of porous magnetite films on carbon steel in high temperature aqueous systems, Corros. Sci. 23 (1983) 295–315.

[32] L. Alamos, Impedance studies of porous electrodes, 35 (1990) 1579–1586.

[33] M.A. Floyd, An Examination of Oxidative Passivated Surfaces on 19th Century Colt Revolver Barrels, (2012).

[34] C.C. Waraksa, G. Chen, D.D. Macdonald, T.E. Mallouk, EIS Studies of Porous Oxygen Electrodes with Discrete Particles, J. Electrochem. Soc. 150 (2003) E429.

[35] L. Angeles, Use of electrochemical impedance spectroscopy for the study of corrosion protection by polymer coatings I ---I I, Appl. Electrochem. 25 (1995) 187–202.

[36] F. Deflorian, L. Fedrizzi, P.L. Bonora, Impedance study of the corrosion protection properties of fluoropolymer coatings, Prog. Org. Coatings. 23 (1993) 73–88.

[37] E. Akbarinezhad, F. Rezaei, J. Neshati, Evaluation of a high resistance paint coating with EIS measurements: Effect of high AC perturbations, Prog. Org. Coatings. 61 (2008) 45–52.

[38] G.W. Walter, The application of impedance methods to study the effects of water uptake and chloride ion concentration on the degradation of paint films--I attached films, 32 (1991) 1059–1084.

[39] H.L.J. (Eds. . S. Haruyama, M. Asari, T. Tsuru, in: M.W. Kendig, Proc. Symp. on Corrosion Protection by Organic Coatings, in: Electrochem. Soc., 1987.

[40] Y. Liu, J. Wang, L. Liu, Y. Li, F. Wang, Study of the failure mechanism of an epoxy coating system under high hydrostatic pressure, Corros. Sci. (2013).

[41] B.R. Hinderliter, S.G. Croll, D.E. Tallman, Q. Su, G.P. Bierwagen, Interpretation of EIS data from accelerated exposure of coated metals based on modeling of coating physical properties, Electrochim. Acta. 51 (2006) 4505–4515.

[42] F. Mansfeld, C.H. Tsai, Determination of Coating Deterioration with EIS I . Basic Relationships, (2010) 3–8.

[43] C.C. Waraksa, G. Chen, D.D. Macdonald, T.E. Mallouk, EIS Studies of Porous Oxygen Electrodes with Discrete Particles, J. Electrochem. Soc. 150 (2003) E429.

[44] G.W. Walter, A review of impedance plot methods used for corrosion preformance analysis of painted metals, Corros. Sci. 26 (1986) 681–703.

[45] E. Akbarinezhad, M. Bahremandi, H.R. Faridi, F. Rezaei, Another approach for ranking and evaluating organic paint coatings via electrochemical impedance spectroscopy, Corros. Sci. 51 (2009) 356–363.

[46] G.W. Walter, The application of impedance methods to study the efects of water uptake and chloride ion concentration on the degradation of paint films, 32 (1991) 1085–1103.